life

MDPI

Article

Lamotrigine Attenuates Lipopolysaccharide-Induced Neuroinflammation, Oxidative Stress, and Apoptosis-Related Marker Changes in the Rat Brain: Evidence from Biochemical, Immunohistochemical, and Molecular Modeling Analyses

Vasudevan Mani [1,*], Minhajul Arfeen [2], Abdullah Saleh Alkhamiss [3] and Ahmad H. Alhowail [1]

[1] Department of Pharmacology and Toxicology, College of Pharmacy, Qassim University, Buraydah 51452, Saudi Arabia; aalhowail@qu.edu.sa
[2] Department of Pharmaceutical Chemistry and Pharmacognosy, College of Pharmacy, Qassim University, Buraydah 51452, Saudi Arabia; m.arfeen@qu.edu.sa
[3] Department of Pathology, College of Medicine, Qassim University, Buraydah 51452, Saudi Arabia; 3772@qu.edu.sa
* Correspondence: v.samy@qu.edu.sa; Tel.: +966-508695644

Abstract

Background and Objective: Lipopolysaccharide (LPS)-induced neuroinflammation is extensively used to model neurodegenerative processes, as it triggers oxidative stress (OS), neuroapoptosis, and inflammatory cascades that contribute to neuronal dysfunction. Beyond its established antiepileptic indication, lamotrigine (LMG) has shown neuroprotective potential, attributed largely to its modulatory effects on oxidative and inflammatory signaling. Here, we examined whether LMG protects rats against LPS-induced neurotoxicity, assessing neuroinflammation, oxidative stress, apoptosis-related markers, and histopathological and immunohistochemical changes. **Methods**: Neuroinflammatory injury was induced by intraperitoneal LPS injection, and LMG was administered orally for 30 days. Brain tissue was then assayed for neuroinflammatory markers (COX-2, TNF-α, IL-6), oxidative stress indices (MDA, GSH, catalase), and apoptotic regulators (Bcl-2, Bax, Caspase-3), with CD45, CD68, BCL-2, and p53 expression additionally profiled by immunohistochemistry. Complementary in silico docking was carried out, placing LMG into Caspase-3, COX-2, Bcl-2, and the TNF-α trimer interface, with co-crystallized ligands used as internal references. **Results**: LPS challenge significantly heightened neuroinflammatory, oxidative, and apoptosis-associated protein levels. COX-2, TNF-α, IL-6, MDA, Bax, and Caspase-3 all rose, while GSH, catalase, and Bcl-2 fell. Consistent with this, LPS-treated brains showed pronounced gliosis with scattered red neurons on histology examination, and immunohistochemistry revealed elevated CD45+ leukocyte infiltration, CD68+ microglial/macrophage activation, and BCL-2/p53 immunopositivity, together pointing to glial activation, immune recruitment, and genomic stress. LMG co-treatment reversed nearly all of these changes: antioxidant capacity was restored, inflammatory and apoptotic responses declined, and fewer CD45-, CD68-, BCL-2-, and p53-positive cells were observed relative to LPS alone. LMG given alone did not significantly alter any biochemical marker relative to the control, although mild gliosis was noted during H&E staining. To explore plausible mechanisms, molecular docking against the targets central to inflammation and apoptosis (Caspase-3, COX-2, Bcl-2, and the TNF-α trimer interface) was performed. The results showed that LMG lacks the required pharmacophore for high-affinity engagement at the COX-2 and Caspase-3 active sites, supporting a predominantly

Academic Editors: Senthil Kumaran Satyanarayanan and Luca Steardo

Received: 23 October 2026
Revised: 22 November 2026
Accepted: 26 November 2026
Published: 29 November 2026

Copyright: © 2026 by the authors. Licensee MDPI, Basel, Switzerland. This article is an open access article distributed under the terms and conditions of the Creative Commons Attribution (CC BY) license.

upstream, transcriptional/signaling-based mechanism at these targets, while LMG showed plausible partial engagement of Bcl-2's BH3 groove P2 subpocket, which may complement the known epigenetic upregulation of Bcl-2 by LMG. Notably, LMG's aromatic scaffold was predicted to interact with the Tyr59/Tyr119/Tyr151 stacking interface of the TNF-α trimer, a computational prediction that warrants experimental validation. Across all four targets, LMG exhibited a marginally lower docking score (~−6.0 to ~8.0 kcal/mol) than the co-crystallized (co-cl) ligands (~−7.5 to 12.3 kcal/mol) but favorable ligand efficiency (LE) relative to the co-cl reference ligands, consistent with a polypharmacological mode of action rather than high-affinity single-target selectivity, warranting further experimental validation of its potential neuroprotective, multi-target pharmacology. **Conclusions**: Building on our previous findings demonstrating LMG-associated preservation of working memory in LPS-challenged rats, the present study investigated whether these neuroprotective effects were accompanied by histopathological and immunohistochemical alterations and explored the underlying molecular interactions through in silico analyses. Collectively, these findings suggest that LMG attenuates LPS-induced neuroinflammation, oxidative stress, and apoptosis-related protein changes, possibly through predominantly indirect mechanisms, with molecular docking predicting additional direct interactions with multiple targets that warrant experimental validation.

Keywords: lamotrigine; microglial activation; inflammation; neuroprotection; immunohistochemistry; molecular docking

1. Introduction

Neurodegeneration describes a process in which neurons progressively lose their structure and function, and many of them eventually die. Clinically, the term covers a large and heterogeneous group of neurological illnesses. These illnesses differ in how they present and in the tissue damage they cause, yet each tends to target particular groups of neurons located in specific areas of the CNS [1]. Neurodegenerative disorders are becoming increasingly prevalent in the United States, with Alzheimer's disease (AD) cases projected to reach 13.8 million by 2050 and Parkinson's disease (PD) incidence rising between 1990 and 2019 [2,3]. Notable examples of such disorders include AD, PD, frontotemporal dementia (FTD), amyotrophic lateral sclerosis (ALS), and Huntington's disease (HD). Despite differences in their underlying pathogenic mechanisms, such as the involvement of specific protein aggregates and genetic alterations, these conditions share several common features [1]. Beyond these common traits, each neurodegenerative disease also has its own clinical and neuropathological profile. Two features recur across the group: some brain areas are damaged far more readily than others, and different proteins aggregate and accumulate abnormally in nerve tissue. The disorders also share chronic inflammation within the CNS [4]. Inflammation is a fundamental pathological response initiated by diverse stimuli that impact biological tissues, such as injury or infection. This response functions as a primary defense mechanism of the body against harmful agents while also facilitating tissue repair and regeneration [5]. In most cases, the immune response is protective and resolves after tissue repair or elimination of the infection; however, if the inflammatory trigger persists, normal resolution mechanisms may fail, leading to chronic inflammation. This ongoing inflammation can promote the release of neurotoxic mediators and worsen neurological disorders. Such persistent stimuli may arise from endogenous sources, such as protein aggregates, or from environmental factors, such as infections, as well as from microbiota changes, aging, diet, or genetic susceptibility [1,4,6]. Environmen-

tal pollution is a further threat to health and contributes substantially to illness and premature death. Airborne particles, heavy metals, and pesticides can all harm the CNS. They do this by promoting oxidative damage and neuroinflammation and by weakening the blood–brain barrier. Over time, this injury may impair cognition and raise the risk of AD and PD, conditions for which effective therapies remain scarce [7] (Figure 1).

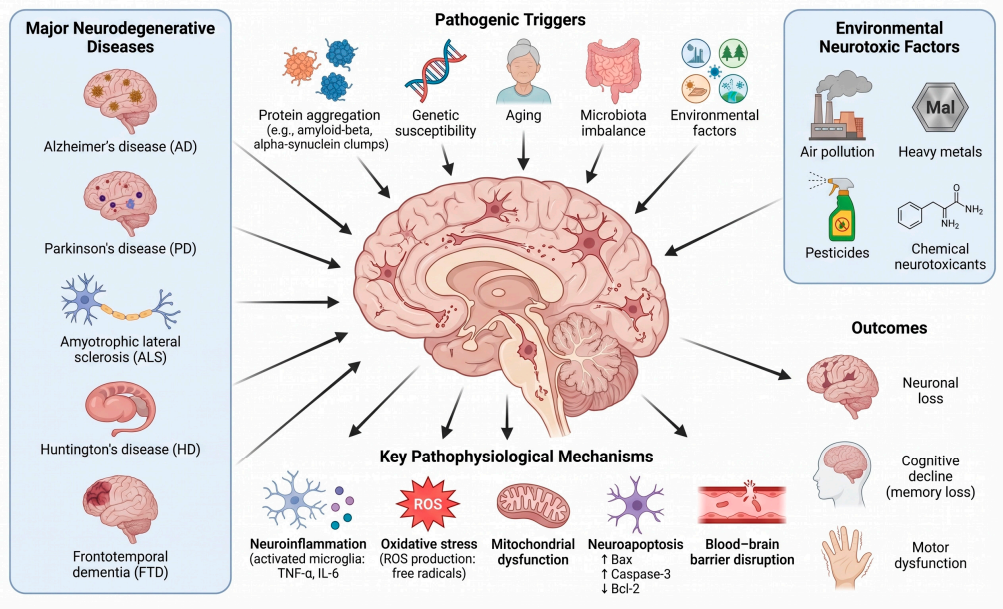


Figure 1. Overview of neurodegeneration and neuroinflammation in CNS disorders. Major diseases include AD, PD, ALS, HD, and frontotemporal dementia. These arise from triggers like protein aggregation, genetics, aging, microbiota imbalance, and environmental factors such as pollution, heavy metals, pesticides, and neurotoxins. These triggers lead to neuroinflammation, oxidative stress, mitochondrial dysfunction, neuroapoptosis, and blood–brain barrier disruption. The end result is neuronal loss accompanied by cognitive and motor decline.

Lamotrigine (LMG) entered clinical use as an antiepileptic agent after US regulatory approval in 1994. It is now prescribed for focal seizures, for the seizures of Lennox–Gastaut syndrome, and for generalized tonic–clonic seizures of primary origin. Approval was broadened in 2003 to include long-term therapy for bipolar I disorder, in which LMG postpones relapse into depression or mania [8]. In epilepsy, LMG is considered a first-line choice for both focal and generalized seizure types, and it is often prescribed with other antiseizure drugs as add-on therapy [9]. Its seizure control is comparable to that of carbamazepine and phenytoin, and patients generally tolerate it better than valproic acid, with fewer side effects [10]. The drug is also used as a mood stabilizer in bipolar disorder. It is most useful for preventing depressive episodes and may help patients who also have anxiety. Some studies have also reported benefit in rapid-cycling forms of the illness [11,12]. LMG is an antiepileptic medication that stabilizes presynaptic neuronal membranes by inhibiting voltage-gated sodium channels and reducing excessive glutamate release [13]. LMG exhibits antioxidant and neuroprotective properties by reducing oxidative stress and enhancing cellular viability. Studies have shown that LMG attenuates oxidative damage while bolstering endogenous antioxidant defenses. Additionally, LMG can suppress microglial activation, thereby reducing neuroinflammation and improving neurological outcomes in experimental models [14–16]. The neuroprotective properties of LMG have been reported in several pathological conditions. Its potential role in spinal cord injury (SCI), particularly in relation to autophagy, a key process involved in maintaining cellular homeostasis, has also been investigated [13]. Both laboratory and clinical

work point to a neuroprotective role for LMG across several disorders of the nervous system [13,17] (Figure 2).

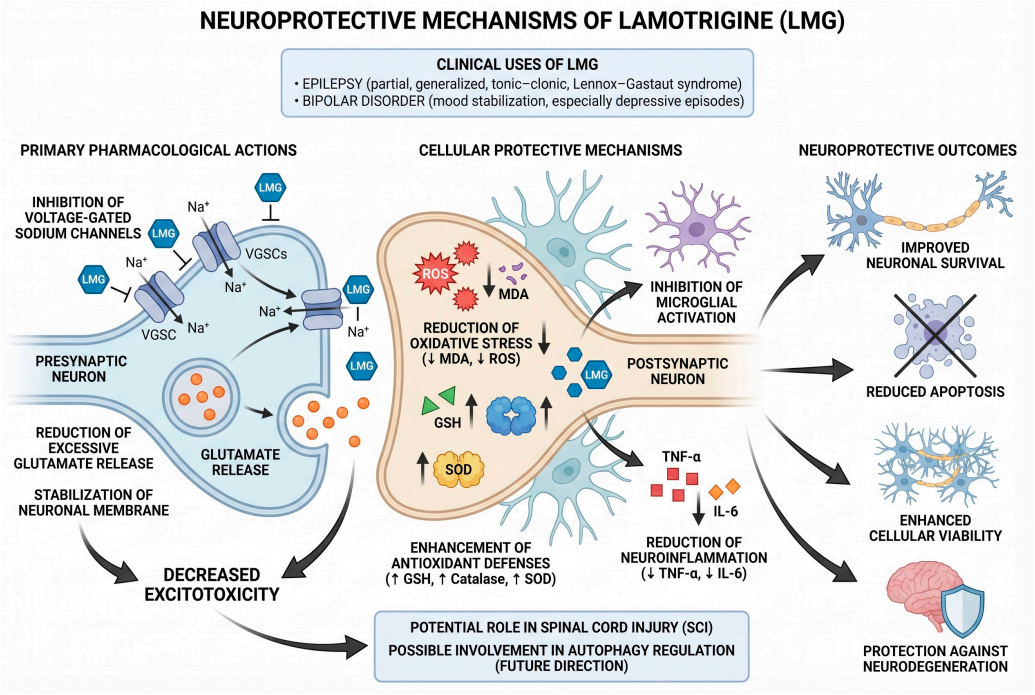


Figure 2. Proposed neuroprotective mechanisms of LMG. LMG inhibits voltage-dependent Na^+ channels, which reduces presynaptic glutamate output, stabilizes the neuronal membrane, and curbs excitotoxicity. In parallel, it lowers oxidative stress, raises antioxidant capacity, and dampens microglial activation and inflammation.

Lipopolysaccharide (LPS) is the endotoxin that forms a major part of the outer membrane of Gram-negative bacteria. Once in the circulation, it provokes a body-wide inflammatory response, chiefly by engaging Toll-like receptor 4 (TLR4). TLRs are one class of pattern recognition receptors (PRRs), and, in the brain, they are present at high levels on microglia and astrocytes. These receptors detect harmful stimuli and rapidly initiate inflammatory responses, leading to microglial activation and the development of neuroinflammation [18]. This cascade ultimately contributes to neuronal degeneration, synaptic damage, and neuronal cell death [19]. The LPS model is widely employed in neuroscience research because neuroinflammation is a central driver of disease in many neurodegenerative conditions, including AD and PD [20]. When LPS is given systemically to rodents, pro-inflammatory cytokine levels rise and the NF-κB pathway is activated. This, in turn, induces inflammatory enzymes such as COX-2 and iNOS. These processes promote neuroinflammation in the cortex and hippocampus, impair cognitive function, and can induce apoptotic cell death in neural and immune cells [21].

Our previous work showed that LMG reduced the working memory deficit produced by LPS in rats, and that this effect coincided with altered levels of neuroinflammatory, oxidative, and apoptotic markers in the prefrontal cortex [21]. Those results gave a first indication that LMG might protect the brain when neuroinflammation is triggered by LPS. However, that study primarily focused on working memory performance and biochemical alterations confined to the prefrontal cortex, and did not characterize the associated histopathological changes, cellular inflammatory responses, or potential molecular interactions underlying these effects. Therefore, the present study, conducted in an independent cohort of animals, extends our previous findings by evaluating the neuroprotective effects of LMG at the whole-brain level, using complementary histopathological and

immunohistochemical approaches, including CD45, CD68, BCL-2, and p53 immunostaining, together with molecular docking analyses. In addition, a longer treatment duration (30 days versus 15 days previously) was employed to provide firmer evidence of its neuroprotective effects against LPS-induced neurotoxicity.

2. Materials and Methods

2.1. Chemicals

LPS was purchased from Sigma-Aldrich (St. Louis, MO, USA) and prepared in 0.9% (*w*/*v*) sodium chloride solution (normal saline), which served as the vehicle for the intraperitoneal injections. LMG tablets (Lamictal® 100 mg; GlaxoSmithKline, Jeddah, Saudi Arabia) were purchased from a retail pharmacy in Saudi Arabia. For oral administration, the tablets were crushed to a fine powder and dispersed in 0.5% (*w*/*v*) carboxymethylcellulose (CMC) to form a uniform suspension delivering 30 mg/kg. Rat-specific ELISA kits for the tissue measurements were obtained from MyBioSource (San Diego, CA, USA).

2.2. Animals

Twenty-four male Wistar albino rats, aged 11–12 weeks and weighing 170–200 g, were obtained from the College of Pharmacy animal unit at Qassim University. The rats were housed three per cage under a 12 h light/dark cycle, with free access to food and drinking water. A 7-day adaptation period preceded dosing, after which the rats were randomly allocated to four equal groups of six. The experimental protocol received approval from the Qassim University Committee of Health Research Ethics (Approval No. 25-18-05). The animals used here constituted an independent cohort; no animals or biochemical data were shared with our previous report [21]. The work was planned and is reported in line with the ARRIVE 2.0 checklist, including the Essential 10 items [22]. Handling and procedures were designed to limit pain and stress to the animals.

We checked the adequacy of six rats per group in two ways: First, a power analysis for a 2 × 2 (two-way) ANOVA was run in G*Power 3.1. Assuming the large LPS effects seen in our earlier work (Cohen's f = 0.75) [21], with α set at 0.05 and numerator df = 1, 24 animals in total gave about 94% power to detect the main effects and the LMG × LPS interaction. Second, using Mead's approach, the error degrees of freedom (24 animals minus 4 groups = 20) fell at the upper end of the accepted 10–20 range.

2.3. Experimental Groups and Treatment Timeline

The four groups (n = 6 each) were treated over 30 days according to the schedule shown in Figure 3. Every rat received a daily oral dose throughout the study, of either the vehicle (0.5% CMC; 0.1 mL/100 g) or LMG (30 mg/kg). During the last four days (days 27–30), each rat also received a daily intraperitoneal (i.p.) injection of either NS or LPS (1 mg/kg). Combining these treatments gave the following groups: CON (oral 0.5% CMC + i.p. NS), LMG (oral LMG + i.p. NS), LPS (oral 0.5% CMC + i.p. LPS), and LMG + LPS (oral LMG + i.p. LPS). Saline injections in the CON and LMG groups ensured that all animals underwent the same injection procedure. The LMG dose was chosen according to earlier reports [23,24]. Four consecutive daily LPS injections (days 27–30, 1 mg/kg i.p.) were used to induce a sustained neuroinflammatory challenge, as repeated daily intraperitoneal LPS at this dose produces a robust and persistent neuroinflammatory, oxidative, and apoptotic response in the rat brain [20,21]. Thus, because LMG dosing commenced on day 1 and continued throughout the subsequent 4-day LPS challenge, the design represents a prophylactic (pretreatment) and concurrent co-treatment paradigm rather than treatment of established neuroinflammation.

In our previous report [21], LMG (30 mg/kg) was given for 15 days. Here, the same dose was kept, but the treatment period was doubled to 30 days, and histopathological, immunohistochemical, and molecular docking endpoints were added. When dosing was complete, the rats were sacrificed and whole brains were removed. Notably, whereas biochemical endpoints in our previous study [21] were assessed in the prefrontal cortex, the present measurements were performed on whole-brain tissue, which was used for both the biochemical and immunohistochemical analyses.

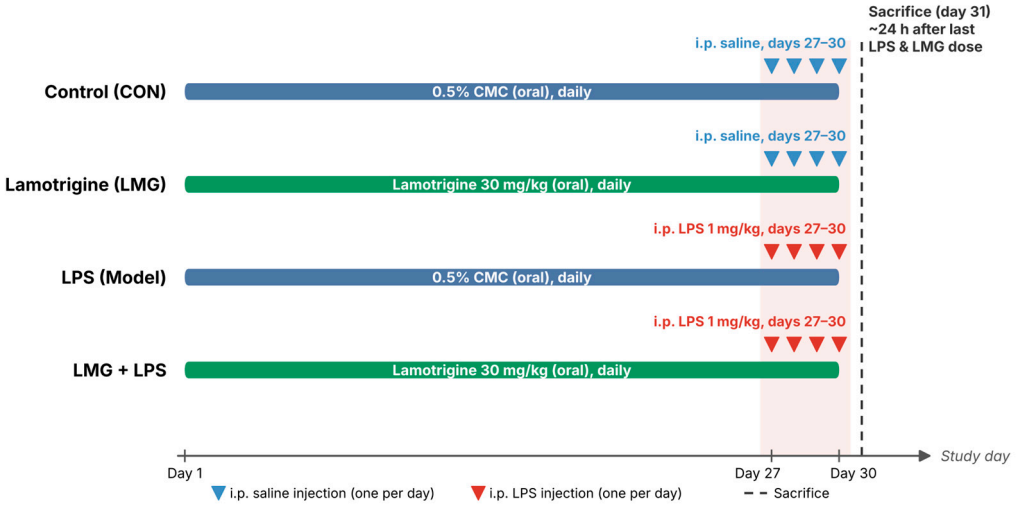


Figure 3. Treatment timeline for the four experimental groups. Twenty-four rats (n = 6/group) were randomized to four arms and dosed over a 30-day period (days 1–30). All rats received a daily oral dose throughout: the CON and LPS groups received 0.5% CMC (0.1 mL/100 g), while the LMG and LMG + LPS groups received oral lamotrigine (30 mg/kg) suspended in 0.5% CMC. During the last four days (days 27–30), each rat received a daily intraperitoneal (i.p.) injection: normal saline in the CON and LMG groups, or LPS (1 mg/kg) in the LPS and LMG + LPS groups. Rats were sacrificed on day 31, approximately 24 h after the final LPS and LMG doses.

2.4. Biomolecular Analysis

2.4.1. Tissue Preparation

Under deep ketamine–xylazine anesthesia (100 and 10 mg/kg, respectively, i.p.), the rats were killed by cervical dislocation. Brains were removed immediately and bisected sagittally. One half was transferred to ice-cold phosphate-buffered saline (pH 7.4; PBS) and disrupted with a motorized tissue homogenizer while kept on ice. After centrifugation (4000 rpm, 10 min), supernatants were collected and frozen at −80 °C for later biochemical assays. Total protein concentration in each supernatant was measured by the biuret colorimetric assay (Crescent Diagnostics, Jeddah, Saudi Arabia), and all biochemical marker levels were normalized to total protein and expressed per mg protein. The remaining half was processed for histology and immunohistochemistry.

2.4.2. Quantification of Inflammatory Mediators

To assess the levels of neuroinflammatory biomarkers, rat-specific ELISA kits based on the double-antibody sandwich methodology were employed. This technique ensures high specificity and sensitivity for biomarker quantification. For the measurement of COX-2 levels, a dedicated ELISA kit was utilized (Catalog No. 266603; assay type: sandwich; detection range: 0.156–10 ng/mL; sensitivity: 0.05 ng/mL). In this assay, microplate wells were pre-coated with monoclonal anti-rat COX-2 antibodies. The wells were subse-

quently incubated with tissue samples and biotin-conjugated detection antibodies, followed by streptavidin–HRP for signal development. Optical density was read at 450 nm, and COX-2 levels in each sample were obtained by interpolation from a standard curve.

TNF-α and IL-6 in the brain supernatants were measured using rat sandwich ELISA kits from the same supplier (TNF-α: Cat. No. 162068, 5–1000 ng/L, detection limit 2.51 ng/L; IL-6: Cat. No. 269892, 15.6–1000 pg/mL, detection limit 5 pg/mL).

2.4.3. Bioassay of Apoptotic Proteins

Three apoptosis-related proteins were assayed in brain homogenates with commercial rat sandwich ELISA kits: BCL-2 (Cat. No. 452319; range 78.1–5000 pg/mL; sensitivity < 30.98 pg/mL), BAX (Cat. No. 2703209; range 0.312–20 ng/mL; sensitivity < 0.125 ng/mL), and Caspase-3 (Cat. No. 261814; range 1.56–100 ng/mL; sensitivity 0.5 ng/mL). These sandwich ELISAs quantify the total protein concentration of each target. For Caspase-3, this reflects the total protein pool and does not distinguish the cleaved, catalytically active fragment or measure caspase enzymatic activity. Samples were added to plates coated with a monoclonal capture antibody against each protein, and bound protein was then detected with a biotin-labeled secondary antibody and an HRP–streptavidin complex. Optical density was read at 450 nm, and the level of each protein was interpolated from its own standard curve. This allowed the pro-apoptotic (BAX, Caspase-3) and anti-apoptotic (BCL-2) arms of the pathway to be compared across groups.

2.4.4. Bioassay of Oxidative Stress Markers

Lipid peroxidation (LPO) and antioxidant defense were evaluated in brain homogenates with commercial kits intended for rat samples. MDA, an LPO product, was measured with a competitive ELISA (Cat. No. 738685; range 50–1000 ng/mL; sensitivity 1.0 ng/mL). In this format, MDA in the sample competes with an HRP-labeled MDA conjugate for a limited number of antibody binding sites, so the signal falls as MDA content rises. GSH was determined colorimetrically (Cat. No. 2540412; range 2–100 μmol/L; sensitivity 2 μmol/L), based on its reaction with 5,5′-dithiobis(2-nitrobenzoic acid) (DTNB) to form a yellow product read on a spectrophotometer. Catalase protein was quantified with a sandwich ELISA (Cat. No. 2704433; range 0.78–50 ng/mL; sensitivity < 0.30 ng/mL), in which an antigen bound to a monoclonal capture antibody on the plate was detected with a biotin-labeled secondary antibody and an HRP–streptavidin complex. Each assay was read at the wavelength recommended by its manufacturer, and sample values were interpolated from the matching standard curve.

2.4.5. Immunohistochemistry

The second section of the brain hemisphere, comprising the cerebrum (cerebral cortex and adjacent parenchyma), was used for histopathology and immunohistochemistry to characterize leukocyte infiltration, microglial activation, apoptotic regulation, and DNA damage at the cellular level. Four markers were selected: CD45 (cluster of differentiation 45), which is expressed on all leukocytes, was used to detect immune cells entering the brain parenchyma, a process that follows loss of blood–brain barrier (BBB) integrity. CD68, a lysosomal protein of phagocytic myeloid cells, served as an index of activated microglia and infiltrating macrophages. The anti-apoptotic protein BCL-2 indicated the capacity of cells to resist apoptotic signals, and the tumor suppressor p53 was used as a marker of DNA damage and cellular stress.

After collection, brain tissues were fixed in 10% neutral buffered formalin for 24 h. Two sections were prepared per animal, and sections from all animals of a group were processed together in group-labeled cassettes. Tissues were dehydrated through a graded ethanol and xylene series, infiltrated with paraffin using an automated tissue processor

(Histo-Tek VP1, Sakura Finetek, Tokyo, Japan), and embedded in paraffin. Sections were cut at 4 μm. One section per block was stained with hematoxylin and eosin on a Tissue-Tek Prisma Plus autostainer (Sakura Finetek, Tokyo, Japan), and the remaining sections were used for immunohistochemistry. Detailed processing and H&E protocols are provided in Tables S1 and S2 (Supplementary Material).

Antibody details, including manufacturer, clone, type, and formulation, are listed in Table 1. Immunohistochemical staining was performed on a Bond-III fully automated system (Leica Biosystems, Melbourne, Australia). Heat-induced epitope retrieval used citrate buffer at pH 6 (CD45, p53) or pH 9 (CD68, BCL-2), with a 20 min primary-antibody incubation at 97 °C. Appropriate positive and negative controls were included in each run to verify staining validity (full protocols in Table S3). Slides were examined at ×400 with a Motic BA410E microscope (Motic, Xiamen, China), by a pathologist blinded to group allocation, and counts were taken in the areas of strongest immunoreactivity (hotspots) in each section. The hotspot method was used because LPS-induced inflammatory changes are focal. Sections were screened at low magnification to identify the area of strongest immunoreactivity, in which positive cells were counted at ×400 [25].

Data are expressed as positive cells per high-power field. Cells were scored as positive when they showed cytoplasmic staining, except for p53, for which only nuclear labeling was counted. Two sections were prepared per animal, and sections from all animals of a group were processed together in group-labeled cassettes; accordingly, the positive-cell counts in Table 2 are reported as representative (semi-quantitative) values per group and were not statistically compared.

Table 1. Primary antibodies used for immunohistochemical staining of rat brain sections. Markers: CD45, infiltrating leukocytes; CD68, activated microglia/macrophages; BCL-2, anti-apoptotic signalling; p53, DNA damage response**.**

Stain	Manufacturer	Concentrated or Ready to Use	Monoclonal or Polyclonal	Clone
CD45	Dako	Ready to Use	Monoclonal	2B11 + PD7/26
CD68	Cell Marque	Ready to Use	Monoclonal	Kp-1
BCL-2	Leica	Ready to Use	Monoclonal	BCL-2/100/D5
p53	Dako	Ready to Use	Monoclonal	DO-7

Table 2. Immunohistochemical scores of CD45, CD68, BCL-2, and p53 in rat brain tissue. Values are the number of positive cells in a single representative high-power field (×400; hotspot area) per group. Because sections from each group were processed together, the counts are semi-quantitative and were not statistically analyzed.

Stain	CON	LMG	LMG + LPS	LPS
CD45	0	3	9	15
CD68	2	3	6	8
BCL-2	0	1	9	11
p53	0	0	17	19

2.5. Statistical Analysis

Results are expressed as mean ± SEM (n = 6 per group). GraphPad Prism 9.5.0 was used for all calculations. Because the four experimental groups constituted a 2 × 2 factorial design, data were analyzed by two-way ANOVA with LMG (vehicle vs. lamotrigine) and LPS (saline vs. LPS) as independent factors, to assess the main effect of each factor and the

LMG × LPS interaction. Where significant effects were detected, pairwise differences between groups were identified using Tukey–Kramer's multiple-comparison test. Statistical significance was set at $p \leq 0.05$.

2.6. Molecular Modeling

2.6.1. Protein and Ligand Preparation

Four ligand-bound protein structures served as docking templates and were sourced from the RCSB Protein Data Bank: cyclooxygenase-2 (COX-2, PDB 5IKR, co-cl with mefenamic acid), Caspase-3 (PDB 3H0E, co-cl with non-peptide inhibitor H0E), Bcl-2 (PDB 6O0K, co-cl with venetoclax), and the TNF-α trimer interface (PDB 2AZ5, co-cl with a trimer-disassembling small molecule SPD-304). Each structure was prepared by retaining only structural waters mediating direct ligand binding site contacts while removing all other crystallographic waters, co-cl ligands, and ions not required for defining the binding site, adding polar hydrogens, and assigning Kollman partial charges. The LMG ligand was downloaded as a 3D SDF file from PubChem (CID 3878). Gasteiger charges were then added and its rotatable bonds were defined. Input files for both the proteins and small molecules (LMG and co-cl ligands) were prepared using AutoDockTools/MGLTools (v1.5.7, La Jolla, CA, USA) [26].

2.6.2. Docking Protocol

Molecular docking was performed using AutoDock Vina (v1.1.2) [27]. A docking search space was centered on the native ligand's binding site for each target, with dimensions of 30 × 30 × 30 Å for COX-2, Bcl-2, and TNF-α. For Caspase-3, a docking search space of 20 × 20 × 20 Å was used. Grid boxes were centered at 38.042, 2.131, 61.28 for COX-2; 24.639, 54.504, 12.6 for Caspase-3; −14.226, 1.146, −10.8 for Bcl-2; and −19.163, 74.451, 33.837 for TNF-α (x, y, z, in Å). Docking was performed using an exhaustiveness value of 8, num_modes = 10, and an energy range of 4 kcal/mol. The lowest-energy (most favorable) conformation was selected for interaction analysis, unless otherwise noted. To check that the docking protocol could reproduce known binding modes, the co-cl ligand of each target was removed and docked back into its original site. The best-scoring redocked pose was then superimposed on the crystal pose, and the RMSD between them was measured in BIOVIA Discovery Studio Visualizer (Dassault Systèmes, San Diego, CA, USA). Redocking validation was performed for all four targets by comparing each docked pose against its corresponding co-crystallized ligand. For Bcl-2 and TNF-α, the native pose was recovered as the top-ranked solution in both cases (RMSD = 0.89 Å and 0.90 Å, respectively), confirming direct agreement between the highest-scoring pose and the crystallographic reference. For COX-2 and caspase-3, the near-native pose was not the top-ranked solution: the RMSD values for the top-ranked and second-ranked poses of the COX-2 native ligand were 1.85 Å and 0.48 Å, respectively, with the near-native pose scoring within 0.5 kcal/mol of the top-ranked pose. For caspase-3, the 2.29 Å pose ranked third of ten generated conformations, scoring within 0.3 kcal/mol of the top-ranked pose. The same near-native caspase-3 pose was reproducibly recovered across grid box sizes of 25, 30, and 40 Å, ranking third, eighth, and fourth of ten generated poses, respectively, with RMSD-to-native values of 2.35, 2.46, and 2.71 Å. Agreement with the native pose improved as box size decreased, consistent with reduced competition from decoy poses outside the binding pocket at smaller search volumes, and the 20 Å box was therefore used for the reported pose. In all four cases, the near-native pose fell within a narrow energy margin of the top-ranked solution, consistent with the known resolution limits of empirical scoring functions in discriminating among closely related binding modes [28,29], and we therefore report best-of-ensemble redocking RMSD, a standard and literature-supported validation convention [30], rather than restricting validation to rank-1 poses alone.

2.6.3. Interaction Analysis

Binding poses were visualized and protein–ligand interactions (hydrogen bonds, ionic/salt bridge contacts, pi stacking, van der Waals and hydrophobic contacts) were identified using the free version of Discovery Studio, with residue numbering taken directly from each deposited PDB structure.

2.6.4. Ligand Efficiency Calculation

To account for the difference in size between LMG and each target's larger co-cl reference ligand, ligand efficiency (LE) was calculated for both LMG and the co-cl ligand at each target using a docking score-based adaptation of the ligand efficiency concept of Hopkins et al. [31]: LE = −ΔG/N (heavy atoms), where ΔG is the predicted binding energy (kcal/mol) obtained directly from docking, retaining its native negative sign for favorable binding, and N (heavy atoms) is the number of non-hydrogen atoms in the ligand. AutoDock Vina reports predicted binding affinities as negative free energy values (kcal/mol), with more negative values indicating more favorable (stronger) predicted binding. This convention is retained for all docking scores reported throughout this study. For the LE calculation specifically, the sign of the docking-derived ΔG is inverted so that LE is expressed as a positive value, consistent with the original ligand efficiency metric of Hopkins et al. [31], in which a larger positive value indicates greater binding energy contributed per heavy atom.

3. Results

3.1. Effect of LMG on Brain Inflammatory Mediators in LPS-Challenged Rats

Because the four groups constitute a 2 × 2 factorial design, brain inflammatory mediators were analyzed by two-way ANOVA with LMG and LPS as independent factors.

Two-way ANOVA for COX-2 revealed a significant main effect of LPS [$F(1,20) = 19.34$, $p < 0.001$], a significant main effect of LMG [$F(1,20) = 11.56$, $p = 0.003$], and a significant LMG × LPS interaction [$F(1,20) = 5.06$, $p = 0.036$], indicating that the effect of LMG on COX-2 depended on the presence of LPS (Figure 4A). Post hoc comparisons showed that COX-2 was elevated by LPS ($p < 0.001$ vs. CON) and significantly reduced by co-treatment with LMG ($p < 0.01$ vs. LPS), whereas LMG alone did not differ from control.

For TNF-α, two-way ANOVA showed significant main effects of LPS [$F(1,20) = 12.89$, $p = 0.002$] and LMG [$F(1,20) = 6.35$, $p = 0.020$], while the LMG × LPS interaction did not reach significance [$F(1,20) = 3.30$, $p = 0.084$] (Figure 4B). Post hoc comparisons confirmed that TNF-α was elevated by LPS ($p < 0.01$ vs. CON) and was significantly lower in the LMG + LPS group than in the LPS group ($p < 0.05$), consistent with an attenuating effect of LMG.

For IL-6, two-way ANOVA revealed significant main effects of LPS [$F(1,20) = 53.88$, $p < 0.001$] and LMG [$F(1,20) = 8.27$, $p = 0.009$], and a significant LMG × LPS interaction [$F(1,20) = 4.92$, $p = 0.038$], indicating that LMG modified the IL-6 response to LPS (Figure 4C). Post hoc comparisons showed that LPS markedly elevated IL-6 ($p < 0.001$ vs. CON) and that co-treatment with LMG significantly reduced it ($p < 0.01$ vs. LPS); however, IL-6 in the LMG + LPS group remained above control levels ($p < 0.05$ vs. CON).

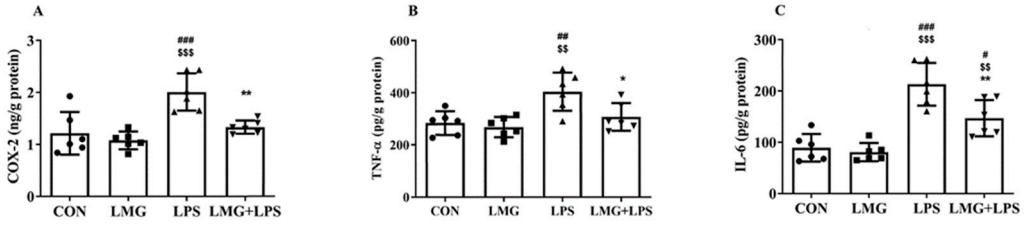


Figure 4. Brain levels of (**A**) COX-2, (**B**) TNF-α, and (**C**) IL-6 in rats treated with LMG, LPS, or both. Bars show mean ± SEM with individual values (n = 6 per group). Data were analyzed by two-way ANOVA (factors: LMG and LPS), followed by Tukey–Kramer's multiple-comparison test. F statistics for the main effects and the LMG × LPS interaction are given in Section 3.1. # $p < 0.05$, ## $p < 0.01$, ### $p < 0.001$ vs. CON; $$ $p < 0.01$, $$$ $p < 0.001$ vs. LMG; * $p < 0.05$, ** $p < 0.01$ vs. LPS.

3.2. Effect of LMG on Brain Apoptotic Markers in LPS-Challenged Rats

For BCL-2, two-way ANOVA revealed significant main effects of LPS [F(1,20) = 50.11, $p < 0.001$] and LMG [F(1,20) = 6.89, $p = 0.016$], and a significant LMG × LPS interaction [F(1,20) = 10.39, $p = 0.004$], indicating that LMG modified the BCL-2 response to LPS (Figure 5A). Post hoc comparisons showed that LPS markedly reduced BCL-2 ($p < 0.001$ vs. CON), and that co-treatment with LMG significantly restored it ($p < 0.01$ vs. LPS); however, BCL-2 in the LMG + LPS group remained below control levels ($p < 0.05$ vs. CON), indicating only partial restoration.

For Bax, two-way ANOVA showed significant main effects of LPS [F(1,20) = 9.70, $p = 0.005$] and LMG [F(1,20) = 5.54, $p = 0.029$], while the LMG × LPS interaction did not reach significance [F(1,20) = 3.44, $p = 0.079$] (Figure 5B). Post hoc comparisons showed that LPS increased Bax ($p < 0.05$ vs. CON) and that co-treatment with LMG significantly reduced it ($p < 0.05$ vs. LPS), returning it to control levels.

For Caspase-3, two-way ANOVA revealed significant main effects of LPS [F(1,20) = 20.38, $p < 0.001$] and LMG [F(1,20) = 14.92, $p = 0.001$], and a significant LMG × LPS interaction [F(1,20) = 12.69, $p = 0.002$], indicating that LMG strongly modified the Caspase-3 response to LPS (Figure 5C). Post hoc comparisons showed that LPS markedly increased Caspase-3 ($p < 0.001$ vs. CON) and that co-treatment with LMG sharply reduced it ($p < 0.001$ vs. LPS), to levels indistinguishable from the control.

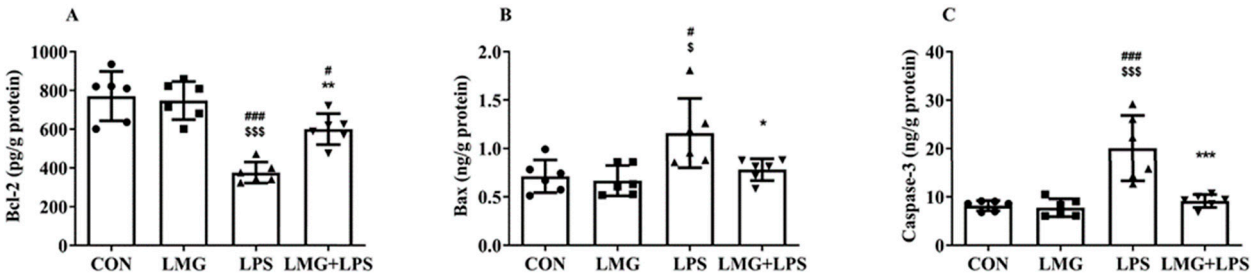


Figure 5. Brain levels of (**A**) Bcl-2, (**B**) Bax, and (**C**) Caspase-3 in rats treated with LMG, LPS, or both. Bars show mean ± SEM with individual values (n = 6 per group). Data were analyzed by two-way ANOVA (factors: LMG and LPS), followed by Tukey–Kramer's multiple-comparison test. F statistics for the main effects and the LMG × LPS interaction are given in Section 3.2. # $p < 0.05$, ### $p < 0.001$ vs. CON; $ $p < 0.05$, $$$ $p < 0.001$ vs. LMG; * $p < 0.05$, ** $p < 0.01$, *** $p < 0.001$ vs. LPS.

3.3. Effect of LMG on Brain Oxidative Stress Markers in LPS-Challenged Rats

For MDA, two-way ANOVA revealed a significant main effect of LPS [F(1,20) = 40.65, $p < 0.001$] and a significant LMG × LPS interaction [F(1,20) = 6.62, $p = 0.018$], while the main effect of LMG approached significance [F(1,20) = 4.14, $p = 0.055$] (Figure 6A). Post hoc comparisons showed that LPS markedly increased MDA ($p < 0.001$ vs. CON) and that co-treatment with LMG reduced it ($p < 0.05$ vs. LPS); however, MDA in the LMG + LPS group remained above control levels ($p < 0.05$ vs. CON), indicating only partial attenuation.

For GSH, two-way ANOVA showed significant main effects of LPS [F(1,20) = 14.75, $p = 0.001$] and LMG [F(1,20) = 9.96, $p = 0.005$], while the LMG × LPS interaction was not significant [F(1,20) = 1.71, $p = 0.205$] (Figure 6B). Post hoc comparisons showed that LPS

depleted GSH ($p < 0.01$ vs. CON) and that co-treatment with LMG significantly restored it ($p < 0.05$ vs. LPS), to levels comparable with the control.

For catalase, two-way ANOVA revealed a significant main effect of LPS [$F(1,20) = 31.71$, $p < 0.001$] and a significant LMG × LPS interaction [$F(1,20) = 8.48$, $p = 0.009$], while the main effect of LMG approached significance [$F(1,20) = 3.90$, $p = 0.062$] (Figure 6C). Post hoc comparisons showed that LPS reduced catalase ($p < 0.001$ vs. CON) and that co-treatment with LMG significantly restored it ($p < 0.05$ vs. LPS), to levels comparable with the control.

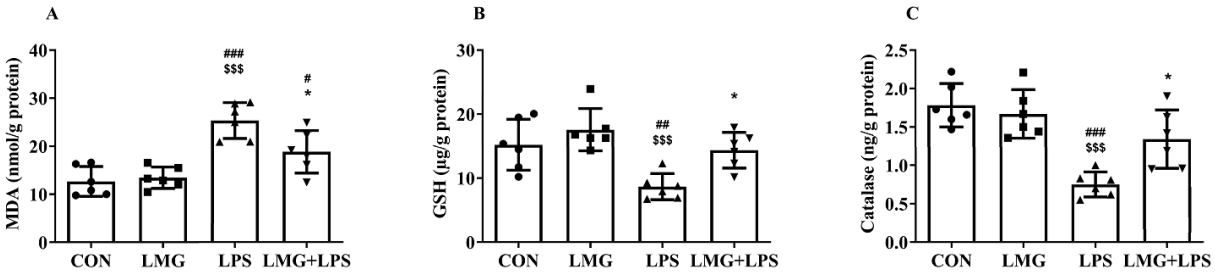


Figure 6. Brain levels of (**A**) MDA, (**B**) GSH, and (**C**) catalase in rats treated with LMG, LPS, or both. Bars show mean ± SEM with individual values ($n = 6$ per group). Data were analyzed by two-way ANOVA (factors: LMG and LPS), followed by Tukey–Kramer's multiple-comparison test. F statistics for the main effects and the LMG × LPS interaction are given in Section 3.3. # $p < 0.05$, ## $p < 0.01$, ### $p < 0.001$ vs. CON; $$$ $p < 0.001$ vs. LMG; * $p < 0.05$ vs. LPS.

3.4. Effect of LMG on Histopathological and Immunohistochemical Changes in LPS-Challenged Rats

Histopathological examination of brain tissue stained with hematoxylin and eosin (H&E) revealed unremarkable brain tissue in the CON group. In the LMG group, there was a mild increase in the number of astrocytes (mild gliosis), whereas the neuronal cells, choroid plexus cells, and blood vessels remained within normal limits. The LPS group showed more pronounced gliosis compared with the LMG group, together with rare red neurons. The LMG + LPS group displayed histopathological features similar to those of the LPS group (Figure 7).

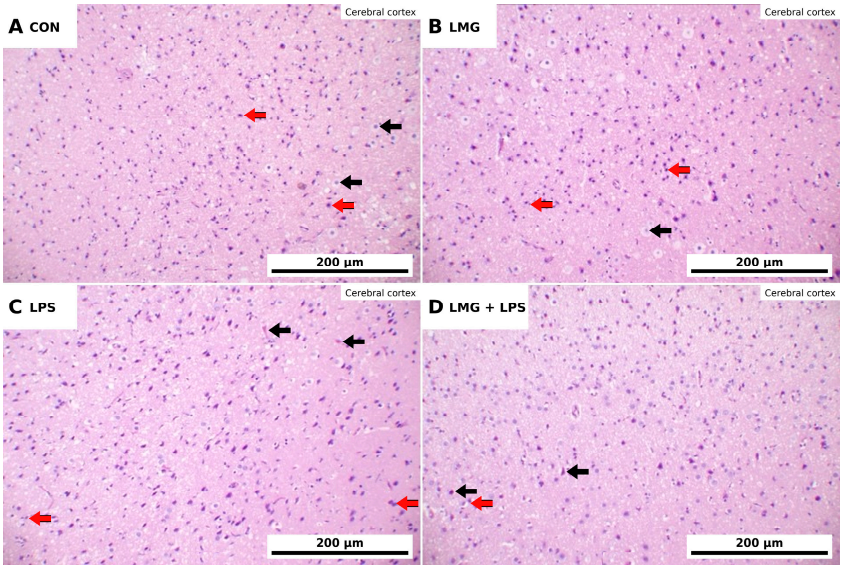


Figure 7. Photomicrographs of H&E-stained sections of the cerebral cortex (magnification ×200; scale bar = 200 µm). (**A**) CON group: normal cerebral tissue showing neurons (black arrows) and

glial cells (red arrows) with unremarkable morphology. (**B**) LMG group: neurons within normal limits (black arrow) with a mild increase in glial cells (mild gliosis; red arrows). (**C**) LPS group: more pronounced gliosis (red arrows) with rare red neurons characterized by eosinophilic cytoplasm and small, dark nuclei (black arrows). (**D**) LMG + LPS group: histopathological features similar to those of the LPS group, with gliosis (red arrow) and red neurons (black arrows).

Immunohistochemical (IHC) analysis was performed to evaluate the expression of CD45, CD68, BCL-2, and p53 across the four experimental groups. The number of positively stained cells for each marker in each group is summarized in Table 2.

CD45 immunostaining was negative in the CON group, indicating the absence of lymphocytes within the normal brain parenchymal tissue, with the exception of those present inside blood vessels. The LMG group showed very few (3) extravasated lymphocytes present between the brain parenchyma. The LPS group showed the highest number of lymphocytes (15) in the brain parenchyma in comparison to the other groups, indicating that the inflammation in the brain of this group was the most severe. In the LMG + LPS group, the inflammation was less severe than in the LPS group, reflected by a lower number of stained lymphocytes (9), although still increased compared with the CON and LMG groups (Figure 8).

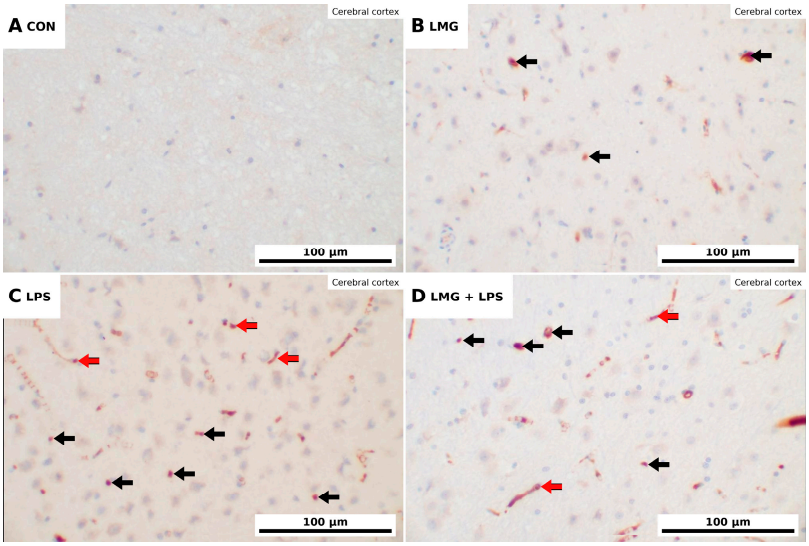


Figure 8. CD45 immunostaining in the cerebral cortex (magnification ×400; scale bar = 100 µm). (**A**) CON: no CD45-positive cells in the brain parenchyma. (**B**) LMG: very few extravasated CD45-positive leukocytes (black arrows). (**C**) LPS: numerous CD45-positive leukocytes in the brain parenchyma (black arrows), in addition to intravascular CD45-positive cells (red arrows). (**D**) LMG + LPS: fewer parenchymal CD45-positive cells than in the LPS group (black arrows), with intravascular CD45-positive cells (red arrows). Arrows indicate representative positive cells. Counts per high-power field (hotspot area) are given in Table 2.

CD68 staining in the CON group showed rare scattered positive cells (2), most likely representing resident microglia/macrophages in the brain parenchyma. The LMG group was similar to the CON group, showing only rare CD68-positive cells (3). The LPS group showed the greatest number of CD68-positive cells (8), suggesting LPS-induced activation and recruitment of microglia/macrophages, with the inflammatory response being most pronounced in this group. Compared with the LPS group, the LMG + LPS group showed fewer CD68-positive cells (6), although the number remained higher than in the CON and LMG groups (Figure 9).

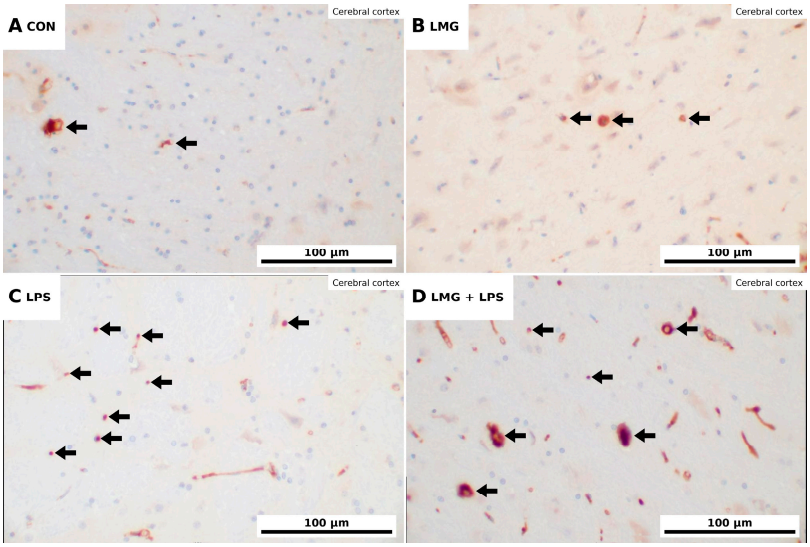


Figure 9. CD68 immunostaining in the cerebral cortex (magnification ×400; scale bar = 100 µm). (**A**) CON and (**B**) LMG: rare CD68-positive microglia/macrophages (black arrows). (**C**) LPS: increased numbers of CD68-positive cells (black arrows). (**D**) LMG + LPS: CD68-positive cells (black arrows), fewer than in the LPS group. Arrows indicate CD68-positive cells. Counts per high-power field (hotspot area) are given in Table 2.

BCL-2 staining was negative in the CON group. The LMG group showed very few BCL-2-positive cells (1). The number of BCL-2-positive cells was greatest in the LPS group (11) among all groups. Compared with the LPS group, the LMG + LPS group showed fewer BCL-2-positive cells (9), although the number remained higher than in the CON and LMG groups (Figure 10). The focal increase in BCL-2-positive cells may reflect a compensatory survival response in stressed cells; however, this interpretation remains hypothetical and requires confirmation.

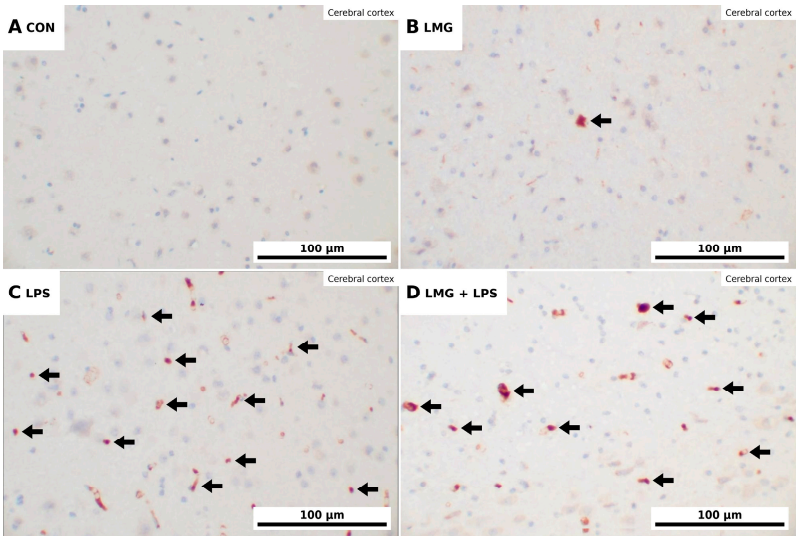


Figure 10. BCL-2 immunostaining in the cerebral cortex (magnification ×400; scale bar = 100 µm). (**A**) CON: no BCL-2-positive cells. (**B**) LMG: a single BCL-2-positive cell (black arrow). (**C**) LPS: numerous BCL-2-positive cells (black arrows). (**D**) LMG + LPS: fewer BCL-2-positive cells than in the LPS group (black arrows). A cell was scored as positive when cytoplasmic staining was visible. Counts per high-power field (hotspot area) are given in Table 2.

p53 immunostaining was negative in the CON group, and the LMG group was similar to the CON group. The LPS group showed numerous p53-positive cells (19), consistent

with activation of a cellular stress/DNA damage response. On morphological grounds, the positive cells were predominantly glial. The LMG + LPS group showed slightly fewer p53-positive cells (17) than the LPS group, although the number remained high (Figure 11).

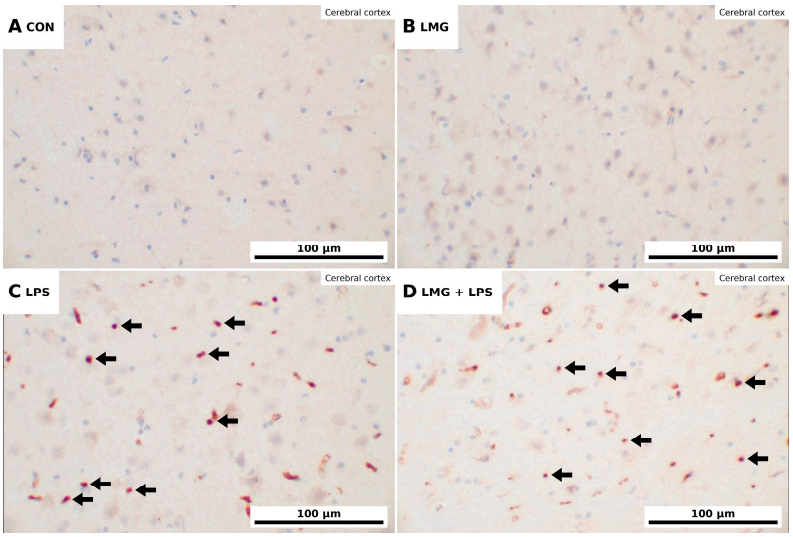


Figure 11. p53 immunostaining in the cerebral cortex (magnification ×400; scale bar = 100 µm). (**A**) CON and (**B**) LMG: no p53-positive cells. (**C**) LPS: numerous p53-positive cells (black arrows). (**D**) LMG + LPS: slightly fewer p53-positive cells than in the LPS group (black arrows). Positivity required nuclear labeling. Arrows indicate representative positive cells, and counts per high-power field (hotspot area) are given in Table 2.

3.5. Binding Interactions of LMG with COX-2, Caspase-3, Bcl-2, and TNF-α

To validate the docking protocol at each target, the native co-cl ligand was extracted and redocked into the active site of its corresponding protein. Redocking reproduced the experimental binding pose with RMSD values of 0.48 Å (COX-2, second-ranked pose), 2.29 Å (Caspase-3, third-ranked pose), 0.89 Å (Bcl-2, top-ranked pose), and 0.90 Å (TNF-α, top-ranked pose), confirming that the docking protocol reliably reproduced the experimentally observed binding geometry at each site. Docking of LMG into the validated binding sites yielded binding energies of −8.1 kcal/mol at COX-2, −5.9 kcal/mol at Caspase-3, −6.9 kcal/mol at Bcl-2, and −6.9 kcal/mol at TNF-α, compared with −8.6, −7.4, −12.3, and −8.7 kcal/mol obtained for the respective co-cl reference ligands (Co-CL) at each site (Table 3). Figure 12 shows the lowest-energy conformations of LMG in the active sites of COX-2, Caspase-3, Bcl-2, and TNF-α. LMG formed a pi–cation interaction with Arg120 and pi–sigma interactions with Ala527 and Leu352, alongside hydrophobic (alkyl/pi–alkyl) contacts with Val116, Val349, Val523, Leu359, and Leu531. At Caspase-3, LMG engaged Tyr204 and Trp206 through pi–sigma interactions and Phe256 through a pi–alkyl contact, formed conventional hydrogen bonds with Thr62 and Ser63, and established a pi–cation interaction with Arg207. At Bcl-2, LMG formed conventional hydrogen bonds with Ala149 and Val133, together with pi–alkyl contacts involving Leu137, Phe104, and Met115. At TNF-α, LMG formed conventional hydrogen bonds with Leu120, Ser60, Gln61, and Tyr151, a van der Waals contact with Gly121, and both pi–pi stacked and amide–pi stacked interactions with Tyr119. Across all four targets, LMG's binding energies were lower in magnitude than those of the respective co-cl reference ligands, and the docked poses were stabilized by a combination of hydrogen bonding, hydrophobic, and aromatic interactions with residues located within the previously characterized binding regions of

each protein. To account for differences in molecular size between LMG and the co-cl reference ligands, ligand efficiency (LE) was calculated. LMG (16 heavy atoms) yielded LE values of 0.51, 0.37, 0.43, and 0.43 kcal/mol/heavy atom at COX-2, Caspase-3, Bcl-2, and TNF-α, respectively, compared with LE values of 0.48 (mefenamic acid, 18 heavy atoms), 0.23 (H0E, 32 heavy atoms), 0.20 (venetoclax, 61 heavy atoms), and 0.22 (SPD-304, 40 heavy atoms) for the corresponding reference ligands. Despite its lower absolute binding energy relative to each reference ligand, LMG exhibited a higher LE than the corresponding reference compound at all four targets.

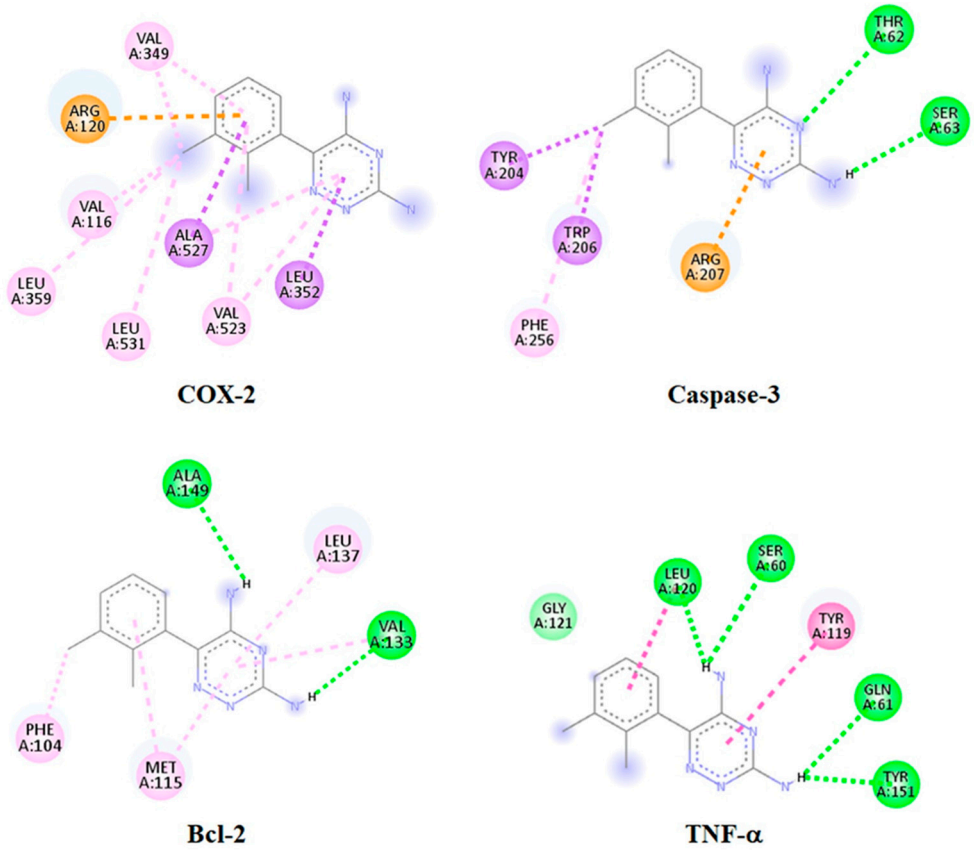


Figure 12. Predicted binding modes of LMG with COX2, Caspase3, Bcl-2, and TNF-α. Hydrogen bonds are shown as green dashed lines, cation–π interactions in orange, and hydrophobic interactions in purple and pink.

Table 3. Docking score of the LMG and the co-cl ligands, RMSD values of the redocked co-cl ligands, and calculated ligand efficiency (LE, docking score/heavy atom) for LMG and the co-cl ligands.

	LMG (Kcal/mol)	co-cl (Kcal/mol)	Redocking RMSD	LMG LE	co-cl LE
COX-2	−8.1	−8.6	0.48	0.51	0.48
Caspase-3	−5.9	−7.4	2.29	0.37	0.23
Bcl-2	−6.9	−12.30	0.89	0.43	0.20
TNF-α	−6.9	−8.7	0.90	0.43	0.22

4. Discussion

Neurodegenerative diseases are a growing global health challenge characterized by progressive neuronal degeneration causing cognitive and motor decline, and their prevalence is expected to rise further due to population aging [32]. Neurodegenerative diseases not only affect patients but also place significant emotional, physical, and financial burdens on caregivers [33]. Moreover, healthcare systems face growing pressure to deliver

adequate care for older individuals with neurodegenerative diseases, often hindered by limited resources, insufficient expertise, and inadequate policy frameworks. In this context, pharmacological interventions represent some of the most direct and clinically applicable strategies for addressing chemical- and drug-induced neurotoxicity [34]. Since toxic neuronal injury often arises from well-defined molecular mechanisms, including oxidative stress, mitochondrial dysfunction, excitotoxicity, inflammation, and apoptosis, therapeutic agents can be specifically developed or repurposed to target these pathways [35]. The goal of pharmacological neuroprotection extends beyond symptom management, aiming to preserve neuronal integrity and function from the earliest stages of damage.

This study extends our earlier work, in which LMG protected rats from LPS-induced deficits in working memory and limited the accompanying inflammatory, oxidative, and apoptotic changes in the prefrontal cortex [21]. That study focused primarily on behavioral working memory performance and biochemical markers. The current investigation addresses complementary aspects of LPS-induced neurotoxicity, including histopathological alterations and immunohistochemical markers of leukocyte infiltration, microglial/macrophage activation, apoptosis, and cellular stress. Notably, these effects were obtained with LMG administered over a longer treatment period, providing further evidence of its neuroprotective action. It should be emphasized that the improvement in working memory was demonstrated in our previous study [21], whereas the present manuscript contains no behavioral data. All histopathological, immunohistochemical, and molecular docking conclusions are drawn exclusively from the current investigation. Importantly, for LMG to exert these central effects, it must access the brain parenchyma. LMG readily crosses the blood–brain barrier and distributes into brain tissue, as shown by its rapid brain uptake and linear plasma–brain relationship in rats [36] and a cerebrospinal fluid-to-serum ratio of ~0.61 at equilibrium [37]. It is also a dual P-glycoprotein/BCRP substrate at the BBB [38]. A detailed pharmacokinetic analysis of brain LMG exposure was beyond the scope of the present study.

Neuroinflammation is a central contributor to neuronal injury in many CNS disorders, with microglia, the resident immune cells of the brain, at its center. Their activation is protective in the short term, but when it persists, it sustains a damaging, chronic inflammatory state [39]. Once activated, microglia release pro-inflammatory mediators such as prostaglandin E2 (PGE2), TNF-α, and IL-6 [40]. Prostaglandin synthesis depends on the cyclooxygenases, and, within the CNS, COX-2 is the predominant, inflammation-coupled isoform [41]. To test whether LMG modifies this inflammatory cascade, we measured COX-2, TNF-α, and IL-6 in brain tissue. All three were highest in LPS-treated rats and were significantly lower when LMG was given alongside LPS, pointing to an anti-inflammatory action of the drug. LMG on its own did not change any of these markers relative to control.

Apoptosis is a regulated, caspase-driven form of cell death that, when it occurs at an abnormal rate, contributes to neuronal loss in neurodegenerative disorders [42]. Caspase-3 acts at the final, executioner stage of the cascade, and its activation signals that cells under severe stress have been committed to death [43]. Further upstream, the balance between pro-apoptotic Bax and anti-apoptotic Bcl-2 determines whether a cell survives or dies, so changes in these proteins reveal which way a toxic insult is tipping that balance [44]. We used Bax, Bcl-2, and Caspase-3 to examine how LMG affects apoptotic signaling in the LPS model. Compared with LPS alone, co-treatment with LMG lowered Bax and Caspase-3 and raised Bcl-2, shifting the balance back toward cell survival. LMG given without LPS left all three proteins at control levels, suggesting that the drug itself does not disturb apoptotic signaling at this dose.

Oxidative stress arises when ROS are generated faster than antioxidant systems can neutralize them, and it is a common mechanism of neurotoxicity and neurodegeneration

[45,46]. Excess ROS damage lipids, proteins, and nucleic acids, leaving measurable products: lipid peroxidation is reflected by MDA, whereas GSH and catalase represent key antioxidant defenses, with catalase detoxifying hydrogen peroxide [46,47]. Here, MDA, GSH, and catalase were used to evaluate the effect of LMG on oxidative stress. Compared with LPS alone, co-treatment with LMG reduced MDA and preserved GSH and catalase. GSH and catalase stayed within the control range, whereas MDA remained somewhat elevated. LMG by itself did not alter any of the three markers, indicating that it does not affect basal redox status at the dose used.

It is noteworthy that LMG did not fully restore IL-6, MDA, and Bcl-2 to control values, in contrast to the near-complete normalization of several other markers. This partial effect likely reflects two factors: The dose and duration used (30 mg/kg, 30 days) may have been submaximal for these endpoints, such that a higher dose or longer pre-treatment might have yielded fuller normalization. In addition, each of these markers is regulated by multiple, partly independent pathways: IL-6 is driven by NF-κB downstream of TLR4 but also by convergent inflammatory signals; MDA is a terminal LPO product that clears more slowly than antioxidant enzymes (GSH, catalase) recover, so residual elevation can persist despite restored antioxidant capacity; and Bcl-2 is subject to transcriptional, epigenetic, and post-translational control by several apoptotic and survival inputs. Incomplete normalization of these specific markers is therefore consistent with a predominantly upstream mechanism of action rather than direct modulation of every endpoint.

The LPS group displayed pronounced alterations during H&E staining, characterized by marked gliosis and rare red neurons, consistent with the established capacity of systemic LPS to activate CNS-resident glia and precipitate neuronal injury through TLR4-mediated signaling [18]. This structural damage was paralleled by the immunohistochemical findings for CD45 and CD68. CD45, a pan-leukocyte marker, is commonly used to identify infiltrating immune cells following disruption of the BBB during neuroinflammatory insults, and its expression rises in proportion to the severity of the underlying inflammatory challenge [48]. Here, CD45-positive cells were almost absent from CON brains and scarce in LMG-treated brains, but were abundant after LPS. Their number was intermediate when LMG was combined with LPS. CD68, which labels phagocytic, pro-inflammatory microglia and macrophages in damaged CNS tissue [49], showed much the same distribution. Fewer CD68-positive cells were observed with LMG + LPS than with LPS alone, a descriptive pattern consistent with the lower TNF-α, IL-6, and COX-2 levels in that group. Together, these data support the view that LMG restrains LPS-driven microglial activation and the influx of immune cells into the brain.

Immunohistochemical staining for BCL-2 further reflected the presence of an active tissue injury response, as the number of BCL-2-positive cells increased progressively from the CON and LMG groups to the LMG + LPS and LPS groups. At first glance, this appears to oppose the ELISA data, in which LPS reduced bulk Bcl-2 concentration. One possible explanation is that the two assays measure different quantities: the ELISA reports the total Bcl-2 protein concentration averaged across a whole-brain homogenate, whereas the IHC score counts cells exceeding a positivity threshold within focal hotspot fields. Although Bcl-2 functions primarily as an anti-apoptotic protein that promotes cell survival by antagonizing Bax [44], we hypothesize that its focal immunohistochemical upregulation in a subset of stressed cells may represent a compensatory survival response by neurons and glia exposed to a pro-inflammatory microenvironment, a localized signal that could diverge from the tissue-averaged concentration measured by ELISA. Differences in spatial scale, in the measured quantity (concentration versus positive-cell count), in the cell populations sampled, and in antibody epitopes between the two assays may all contribute to the apparent discrepancy; however, this explanation remains hypothetical, as the present study did not include experiments designed to resolve it, such as region-specific protein

analysis or co-localization of Bcl-2 with cell type markers. Similarly, the fewer Bcl-2-positive cells observed in the LMG + LPS group relative to the LPS group may reflect a reduced cellular stress burden under LMG, while the partial recovery of bulk Bcl-2 concentration by ELISA suggests improved net survival signaling. Given the descriptive nature of the IHC data, this interpretation also requires confirmation. We acknowledge, however, that cell type-specific double-labeling or an independent quantitative method would be needed to definitively resolve the cellular origin of these signals, which we identify as a direction for future study. Finally, p53 immunostaining, which reflects activation of the DNA damage response and the guardian-of-the-genome function of this tumor suppressor protein [50], was undetectable in the CON and LMG groups but markedly elevated in the LMG + LPS and LPS groups, indicating that LPS-induced injury was sufficient to trigger a genomic stress response in brain parenchymal cells. The slightly lower number of p53-positive cells observed in the LMG + LPS group compared with the LPS group may indicate a modest attenuation of this stress response by LMG, although this descriptive difference should be interpreted with caution. Collectively, the immunohistochemical findings are consistent with the biochemical evidence and suggest that LMG attenuates LPS-induced microglial activation and leukocyte infiltration in the rat brain. In contrast, H&E staining did not show a clear histopathological improvement with LMG, as the LMG + LPS group displayed features similar to those of the LPS group. The evidence for LMG-associated protection in this study therefore derives primarily from the biochemical and immunohistochemical data. LMG alone produced mild gliosis but no other histopathological alteration relative to the control group.

The results from the in vivo study show that LMG co-treatment reverses the LPS-induced increases in neuroinflammatory markers (COX-2, TNF-α, IL-6), the oxidative stress marker MDA, and the pro-apoptotic regulators Bax and Caspase-3; restores GSH, catalase, and Bcl-2; and is associated with fewer CD45-, CD68-, and p53-positive cells. These findings reflect prophylactic neuroprotection, as lamotrigine was present before and throughout the inflammatory insult. To probe whether these effects could plausibly arise from direct physical engagement of the corresponding proteins rather than exclusively from upstream transcriptional or signaling modulation, molecular docking was performed against four proteins central to these pathways: Caspase-3, COX-2, Bcl-2, and the TNF-α trimer interface (the structure defining the small-molecule TNF-α disassembly pocket).

Across the four targets, LMG's docking scores ranged narrowly from −5.9 to −8.1 kcal/mol, with COX-2 yielding the most favorable score, Caspase-3 the least favorable, and Bcl-2 and TNF-α falling in between. It is notable that this ranking does not fully parallel the qualitative interaction analysis described below. COX-2 achieved the most negative score despite lacking the canonical ionic anchor interaction, which likely reflects the cumulative contribution of multiple hydrophobic contacts accumulated along its relatively long, enclosed substrate channel rather than a single dominant, high-specificity interaction. This underscores an important caveat in interpreting docking scores in isolation: a favorable total score can arise from the additive effect of numerous modest contacts distributed across a ligand's surface, and does not necessarily indicate the presence of a strong, mechanistically decisive interaction of the kind that defines high-affinity, target-selective binding [28,51]. Taken together, the relatively narrow and moderate range of docking scores observed across all four targets is more consistent with LMG acting as a modest-affinity ligand capable of engaging multiple components of the neuroinflammatory and apoptotic pathway to a comparable degree, rather than exhibiting high-affinity, single-target selectivity, a pattern in line with a polypharmacological mode of action rather than a dominant primary target [52,53].

An additional consideration when interpreting the absolute docking scores is the substantial size difference between LMG and each of the co-cl reference ligands, all of which are considerably larger, more elaborated molecules optimized through extensive structure–activity relationship campaigns. Because docking scoring functions generally scale with the number of favorable atomic contacts a ligand can make, larger molecules inherently tend to achieve more negative total binding energies regardless of how efficiently each individual atom contributes to binding. To account for this, ligand efficiency (binding energy normalized per heavy atom) was calculated, and LMG was found to exhibit a higher ligand efficiency than the corresponding reference ligand at all four targets, despite its consistently lower absolute binding energy. This finding is consistent with the principles underlying fragment-based drug discovery, in which a small molecule's high per-atom efficiency, rather than its absolute potency, is considered the more meaningful indicator of a productive starting scaffold [31,54]. Viewed in this light, LMG's docking profile across Caspase-3, COX-2, Bcl-2, and TNF-α is more appropriately interpreted not as evidence of weak or negligible target engagement, but as the expected signature of a compact molecule occupying a fraction of each binding site efficiently, raising the possibility that structural elaboration of the LMG scaffold, guided by the specific subpocket interactions identified here, could yield analogs with improved absolute affinity while retaining or improving upon this per-atom efficiency.

Docking of LMG into the COX-2 active site channel showed that the ligand occupied a hydrophobic substrate channel, forming van der Waals/pi–alkyl contacts with channel-lining residues and reaching the channel entrance, where Arg120, the residue that anchors the carboxylate group of essentially all classical NSAIDs, engaged LMG only through a weak pi–cation interaction rather than the canonical ionic salt bridge [55]. Because LMG possesses no carboxylic acid or carboxylate-mimetic group, it cannot reproduce the anchoring interaction that defines high-affinity, direct COX-2 active site inhibition. This fits with earlier reports that long-term LMG treatment lowers both COX-2 mRNA and COX-2 protein in the rat frontal cortex. It also fits with evidence that the drug interrupts NMDA receptor-triggered arachidonic acid release, a step that precedes COX-2 induction [56,57]. LMG may therefore reduce COX-2 indirectly, by acting on its expression and upstream signaling. Taken together, the docking result argues against LMG acting as a direct, high-affinity COX-2 active site inhibitor, and instead supports a model in which the COX-2 normalization observed in the LPS model is driven predominantly by upstream transcriptional suppression of COX-2 expression and interruption of the arachidonic acid signaling cascade that induces it, rather than by direct enzymatic blockade.

Docking against the Caspase-3 active site placed LMG's dichlorophenyl ring within the S4 hydrophobic/aromatic subpocket (contacts with Tyr204, Trp206, and Phe256), with the triazine head group forming hydrogen bonds to Thr62/Ser63 and a pi–cation interaction with Arg207. Arg207, together with Arg64, Gln161, and Ser205, forms the S1 aspartate recognition pocket that gives Caspase-3 its strict substrate specificity. Every validated Caspase-3 inhibitor engages this pocket through an ionic network [58,59]. As with COX-2, LMG's lack of an acidic warhead means it can only approximate this anchoring interaction through a weaker, non-ionic substitute. This is consistent with, and helps explain, the earlier reported finding that LMG suppresses proteasome inhibitor-induced Caspase-3 activation by acting upstream, blocking the mitochondrial and Caspase-8/Bid-dependent signaling pathways that trigger Caspase-3 cleavage, rather than through direct inhibition of the Caspase-3 enzyme itself [60]. The docking data therefore support a model in which the reduced Caspase-3 activity observed in the LPS neuroinflammation model reflects LMG's suppression of upstream apoptotic signaling, with any direct active site engagement representing, at most, a modest auxiliary contribution rather than the primary mechanism.

Docking against Bcl-2 placed LMG within the P2 hydrophobic subpocket of the BH3-binding groove, the same subpocket historically used as the initial anchor point in fragment-based discovery campaigns that ultimately produced ABT-737 and venetoclax, where it was predicted to form hydrogen bonds (to the backbone near Ala149 and Val133) alongside hydrophobic contacts with Phe104, Met115, and Leu137 [61–63]. Unlike the COX-2 and Caspase-3 results, this pose does not rely on a weakened substitute for a missing ionic interaction; it reflects chemically appropriate contacts within a validated druggable subpocket, though without extending across the full BH3 groove to engage the ionic anchor (the arginine that mimics the natural BH3 peptide's conserved aspartate) that defines full-potency BH3-mimetic binding. This is consistent with a fragment-like, partial engagement of the groove. Combined with the previously reported finding that LMG upregulates Bcl-2 transcriptionally through HDAC inhibition and histone acetylation at the Bcl-2 promoter [64], this docking result raises the plausible, complementary possibility that LMG may also directly and partially engage the Bcl-2 protein itself, potentially contributing an additional, protein-level stabilizing effect on top of its transcriptional upregulation of Bcl-2 expression, thus offering a two-tiered explanation (transcriptional plus partial direct engagement) for the Bcl-2/Bax rebalancing observed in the LPS model.

The most notable docking result was obtained against the TNF-α trimer interface pocket (PDB 2AZ5, validated to 0.89 Å RMSD). Unlike the ionic anchor-dependent pockets of COX-2, Caspase-3, and Bcl-2, this pocket's defining structural feature is an aromatic stacking interface formed by Tyr59, Tyr119, and Tyr151 at the center of the native trimer, which the small-molecule inhibitor SPD-304 exploits to destabilize the trimer and promote dissociation into an inactive dimer [65]. In the docking pose, LMG, itself an aromatic, bicyclic ring-bearing molecule was predicted to engage this exact residue cluster directly, forming predicted pi–pi stacking and amide–pi stacking contacts with Tyr119, together with predicted hydrogen bonds to Ser60 and Gln61/Tyr151 and a van der Waals contact with Gly121. This is mechanistically distinct from the other three targets: rather than substituting a weaker interaction for a missing chemical feature, LMG's own aromatic character is directly compatible with the type of interaction (pi stacking) that defines this specific pocket's pharmacology. This raises a genuinely novel mechanistic hypothesis not previously reported in the literature: LMG may be capable of directly engaging the same TNF-α trimer interface pocket exploited by dedicated TNF-α-disassembling small molecules, potentially contributing directly to TNF-α inactivation rather than acting solely through downstream transcriptional or signaling effects. It is important to note, however, that static docking demonstrates structural and chemical compatibility with the already dissociated, compound-bound dimer conformation captured in the crystal structure; it cannot demonstrate that LMG possesses the potency required to actively drive trimer dissociation, which is a dynamic, kinetically demanding conformational event that would require independent biophysical validation (e.g., analytical ultracentrifugation, dissociation kinetics assays, or TNF-α bioactivity assays) to confirm.

Taken together, the four docking results support a multi-tiered, polypharmacology-consistent explanation for LMG's neuroprotective effect in the LPS-induced neuroinflammation model, rather than a single unifying direct target. At COX-2 and Caspase-3, the docking data argue against potent direct active site inhibition—LMG lacks the acidic pharmacophore required for high-affinity engagement at either site—and instead support a model in which these two arms of the phenotype (reduced COX-2 activity, reduced Caspase-3-associated pro-apoptotic signaling) are mediated predominantly through the previously established upstream mechanisms: transcriptional downregulation of COX-2 expression and interruption of the arachidonic acid cascade, and suppression of the mitochondrial/Caspase-8-dependent signaling that activates Caspase-3, respectively. At Bcl-2, the docking data support a two-tiered model combining the known epigenetic (HDAC-

mediated) transcriptional upregulation with a plausible, complementary partial direct engagement of the BH3 groove's P2 subpocket. At the TNF-α trimer interface, the molecular docking yielded the most notable computational prediction of a possible direct interaction, with LMG's aromatic scaffold predicted to engage the same Tyr–Tyr–Tyr stacking interface exploited by dedicated TNF-α inhibitors, a novel hypothesis meriting dedicated experimental follow-up. It should be noted that this docking panel did not address several other markers reported in the LPS neuroinflammation dataset. IL-6, the oxidative stress indices (MDA, GSH, catalase), and p53 immunopositivity and their normalization by LMG are most parsimoniously explained as a downstream consequence of the upstream anti-inflammatory and anti-apoptotic effects addressed above (e.g., IL-6 transcription lies downstream of the same NF-κB axis triggered by TLR4/LPS signaling that also drives COX-2 and TNF-α expression) rather than through a distinct, independently validated direct mechanism. Future docking work targeting the TLR4/MD-2 LPS recognition complex, the Keap1/Nrf2 antioxidant response interface, and the MDM2–p53 interaction could extend this mechanistic picture to the remaining, currently unaddressed components of the phenotype.

Several limitations should be acknowledged: First, the prophylactic/co-treatment design does not address whether LMG can reverse already established neuroinflammation; a post-LPS therapeutic paradigm would be required to test this. Second, LMG exposure (plasma/brain concentrations) and peripheral inflammatory responses were not measured, so the direct central actions of LMG cannot be fully separated from secondary effects of systemic LPS. Third, the brains were not transcardially perfused; although the tissue was washed and the supernatant cleared by centrifugation, a residual intravascular contribution, particularly to CD45 staining, cannot be excluded, though the identical procedure across groups makes it unlikely to explain the between-group differences. Fourth, apoptosis was inferred from total BAX, BCL-2, and Caspase-3 levels measured by ELISA; cleaved Caspase-3 and direct assays such as TUNEL were not performed, so these data reflect apoptosis-associated protein changes rather than confirmed neuronal apoptosis. Fifth, immunohistochemical quantification was semi-quantitative: because sections from all animals of a group were processed together, individual sections could not be assigned to specific animals, and positive cells were counted in a single hotspot field per group. These counts could therefore not be analyzed statistically and are presented as descriptive observations that support, but do not independently establish, the biochemical findings. Future studies will incorporate per-animal quantification across multiple fields with formal statistical analysis. Sixth, histopathological (H&E) assessment was qualitative; absolute quantification of neuronal loss and gliosis was not performed, and the LPS and LMG + LPS groups showed broadly similar features. Quantitative or stereological histopathological scoring is recommended for future studies.

5. Conclusions

The present study provides compelling evidence that LPS-induced neurotoxicity triggered significant neuroinflammation, OS, and apoptosis-associated protein changes, accompanied by gliosis and occasional red neurons, in a rat model. LPS exposure resulted in marked elevations in pro-inflammatory mediators, including COX-2, TNF-α, and IL-6, confirming the activation of neuroinflammatory pathways. In parallel, oxidative stress analysis revealed a significant increase in LPO, as indicated by elevated MDA levels, accompanied by a reduction in key antioxidant defenses, including GSH and catalase. Furthermore, apoptotic signaling was substantially dysregulated, as evidenced by increased expression of pro-apoptotic markers Bax and Caspase-3, along with a reduction in the anti-apoptotic marker Bcl-2, indicating a shift in apoptosis-associated regulatory proteins

toward a pro-apoptotic balance. Histopathological examination (H&E) confirmed LPS-induced injury, with pronounced gliosis and rare red neurons in the LPS group, while immunohistochemistry showed increased CD45-positive leukocyte infiltration, CD68-positive microglial/macrophage activation, and elevated BCL-2 and p53 immunopositivity, indicating leukocyte recruitment, glial activation, and a genomic stress response. During H&E staining, the LPS and LMG + LPS groups showed broadly similar features; accordingly, the evidence for LMG-associated protection derived primarily from the biochemical findings, supported descriptively by the immunohistochemical observations. LMG administration significantly reduced neuroinflammatory cytokines, restored antioxidant balance, and modulated apoptotic pathways by decreasing Bax and Caspase-3 while increasing Bcl-2 expression, while fewer CD45-, CD68-, BCL-2-, and p53-positive cells were observed relative to the LPS group. These findings suggest that LMG protects against LPS-induced neuroinflammatory, oxidative, and apoptosis-related changes by targeting multiple interconnected molecular and cellular mechanisms. Notably, LMG alone did not significantly alter any biochemical marker compared with the control group, although mild gliosis was observed during H&E staining. Dedicated safety studies would be required to establish its safety profile. Molecular docking suggested that LMG's neuroprotective effect may plausibly arise from a combination of indirect (upstream transcriptional/signaling) and partial direct target engagement mechanisms, rather than a single dominant target, although this computational model requires experimental validation. The docking data are consistent with a polypharmacology-based, multi-tiered model of LMG's neuroprotection. The predicted TNF-α trimer interface engagement stands out as the most mechanistically novel finding and the one most warranting dedicated experimental follow-up using SPR, ITC, or cellular models. Overall, the biochemical and immunohistochemical findings suggest that LMG attenuates inflammation-driven neurotoxicity and oxidative damage, although no clear improvement in tissue morphology was observed during H&E staining. These findings suggest that LMG may represent a promising therapeutic candidate for neurodegenerative disorders associated with chronic neuroinflammation and oxidative stress. Future studies including experimental validation of the computationally predicted direct TNF-α and Bcl-2 interactions (e.g., biophysical binding assays) are warranted to further elucidate its molecular mechanisms and evaluate its long-term efficacy and clinical applicability.

Supplementary Materials: The following supporting information can be downloaded at https://www.mdpi.com/article/10.3390/life16122043/s1: Table S1: Automated tissue-processing protocol (Histo-Tek VP1 tissue processor, Sakura); Table S2: Hematoxylin and eosin (H&E) staining protocol (Tissue-Tek Prisma Plus autostainer, Sakura); Table S3: Immunohistochemistry antibody specifications and protocols (Bond-III fully automated IHC system, Leica).

Author Contributions: Conceptualization, V.M., M.A., A.S.A. and A.H.A.; methodology, V.M., M.A., A.S.A. and A.H.A.; software, V.M. and M.A.; validation, V.M. and M.A.; formal analysis, V.M., M.A., A.S.A. and A.H.A.; investigation, V.M., M.A. and A.S.A.; resources, V.M., M.A. and A.S.A.; data curation, V.M., M.A., A.S.A. and A.H.A.; writing—original draft preparation, V.M., M.A. and A.S.A.; writing—review and editing, V.M., M.A. and A.H.A.; visualization, V.M.; supervision, V.M.; project administration, V.M.; funding acquisition, V.M. and A.S.A. All authors have read and agreed to the published version of the manuscript.

Funding: The Researchers would like to thank the Deanship of Graduate Studies and Scientific Research at Qassim University (https://www.qu.edu.sa) for financial support (QU-APC-2026).

Institutional Review Board Statement: All the experimental procedures of the present study were conducted according to the relevant guidelines and approved by the Committee of Research Ethics,

Deanship of Graduate Studies and Scientific Research, Qassim University, under research proposal number 25-18-05 dated 22 December 2025.

Informed Consent Statement: Not applicable.

Data Availability Statement: The data presented in this study are available in the article; further inquiries can be directed to the corresponding author.

Acknowledgments: The Researchers would like to thank the Deanship of Graduate Studies and Scientific Research at Qassim University (https://www.qu.edu.sa) for financial support (QU-APC-2026). During the preparation of this manuscript, the authors used ChatGPT (GPT-5.3, OpenAI) for the purposes of improving the readability and language of the manuscript. The authors have reviewed and edited the output and take full responsibility for the content of this publication.

Conflicts of Interest: The authors declare no conflicts of interest.

Abbreviations

The following abbreviations are used in this manuscript:

AD	Alzheimer's disease
ALS	Amyotrophic lateral sclerosis
Bax	Bcl-2-associated X protein
Bcl-2	B-cell lymphoma 2
CD45	Cluster of differentiation 45
CD68	Cluster of differentiation 68
COX-2	Cyclooxygenase-2
FTD	Frontotemporal dementia
GSH	Reduced glutathione
HD	Huntington's disease
IHC	Immunohistochemistry
IL-6	Interleukin-6
iNOS	Inducible nitric oxide synthase
LMG	Lamotrigine
LPS	Lipopolysaccharide
MDA	Malondialdehyde
NF-κB	Nuclear factor kappa B
PD	Parkinson's disease
PDB	Protein Data Bank
PRRs	Pattern recognition receptors
ROS	Reactive oxygen species
TLR4	Toll-like receptor 4
TNF-α	Tumor necrosis factor alpha

References

1. Zhang, W.; Xiao, D.; Mao, Q.; Xia, H. Role of neuroinflammation in neurodegeneration development. *Signal Transduct. Target. Ther.* **2023**, *8*, 267. https://doi.org/10.1038/s41392-023-01486-5.
2. Ou, Z.; Pan, J.; Tang, S.; Duan, D.; Yu, D.; Nong, H.; Wang, Z. Global trends in the incidence, prevalence, and years lived with disability of Parkinson's disease in 204 countries/territories from 1990 to 2019. *Front. Public Health* **2021**, *9*, 776847. https://doi.org/10.3389/fpubh.2021.776847.
3. Zhang, X.X.; Tian, Y.; Wang, Z.T.; Ma, Y.H.; Tan, L.; Yu, J.T. The epidemiology of Alzheimer's disease modifiable risk factors and prevention. *J. Prev. Alzheimers Dis.* **2021**, *8*, 313–321. https://doi.org/10.14283/jpad.2021.15.
4. Hammond, T.R.; Marsh, S.E.; Stevens, B. Immune signaling in neurodegeneration. *Immunity* **2019**, *50*, 955–974. https://doi.org/10.1016/j.immuni.2019.03.016.
5. Li, K.; Chen, R.; Wang, R.; Fan, W.; Zhao, N.; Yang, Z.; Yan, J. Neuroinflammation in neurodegenerative diseases: Focusing on the mediation of T lymphocytes. *Neural Regen. Res.* **2026**, *21*, 1864–1889. https://doi.org/10.4103/NRR.NRR-D-24-01539.

6. Mou, Y.; Du, Y.; Zhou, L.; Yue, J.; Hu, X.; Liu, Y.; Chen, S.; Lin, X.; Zhang, G.; Xiao, H.; et al. Gut microbiota interact with the brain through systemic chronic inflammation: Implications on neuroinflammation, neurodegeneration, and aging. *Front. Immunol.* **2022**, *13*, 796288. https://doi.org/10.3389/fimmu.2022.796288.
7. Nabi, M.; Tabassum, N. Role of environmental toxicants on neurodegenerative disorders. *Front. Toxicol.* **2022**, *4*, 837579. https://doi.org/10.3389/ftox.2022.837579.
8. Ali, D.N.; Campbell, I.H.; Leung, J.G.; Gonzalez Campos, T.; Liu, D.; Ercis, M.; Markota, M.; Ceylan, D.; Lara-Breitinger, K.; Lopez-Jimenez, F.; et al. Clinical insights into the mechanistic crossroads of lamotrigine and therapeutic ketosis in bipolar depression. *Biol. Psychiatry Glob. Open Sci.* **2025**, *6*, 100616. https://doi.org/10.1016/j.bpsgos.2025.100616.
9. Compagno Strandberg, M.; Söderberg-Löfdal, K.; Kimland, E.; Dahlin, M.; Källén, K. Evidence-based anti-seizure monotherapy in newly diagnosed epilepsy: A new approach. *Acta Neurol. Scand.* **2020**, *142*, 323–332. https://doi.org/10.1111/ane.13312.
10. Costa, B.; Vale, N. Understanding lamotrigine's role in the CNS and possible future evolution. *Int. J. Mol. Sci.* **2023**, *24*, 6050. https://doi.org/10.3390/ijms24076050.
11. Miller, J.N.; Black, D.W. Bipolar disorder and suicide: A review. *Curr. Psychiatry Rep.* **2020**, *22*, 6. https://doi.org/10.1007/s11920-020-1130-0.
12. Żełabowski, K.; Wojtysiak, K.; Ratka, Z.; Biedka, K.; Chłopaś-Konowałek, A. Lamotrigine therapy: Relation between treatment of bipolar affective disorder and incidence of Stevens-Johnson syndrome—A narrative review of the existing literature. *J. Clin. Med.* **2025**, *14*, 4103. https://doi.org/10.3390/jcm14124103.
13. Zhang, M.; Chen, L.; Gao, H.; Liu, T. Lamotrigine enhances autophagy and reduces post-traumatic spinal neural injury in mice. *J. Integr. Neurosci.* **2025**, *24*, 37357. https://doi.org/10.31083/JIN37357.
14. Arora, T.; Mehta, A.K.; Sharma, K.K.; Mediratta, P.K.; Banerjee, B.D.; Garg, G.R.; Sharma, A.K. Effect of carbamazepine and lamotrigine on cognitive function and oxidative stress in brain during chemical epileptogenesis in rats. *Basic Clin. Pharmacol. Toxicol.* **2010**, *106*, 372–377. https://doi.org/10.1111/j.1742-7843.2009.00499.x.
15. Faustmann, T.J.; Corvace, F.; Faustmann, P.M.; Ismail, F.S. Effects of lamotrigine and topiramate on glial properties in an astrocyte-microglia co-culture model of inflammation. *Int. J. Neuropsychopharmacol.* **2022**, *25*, 185–196. https://doi.org/10.1093/ijnp/pyab080.
16. Kośmider, K.; Kamieniak, M.; Czuczwar, S.J.; Miziak, B. Second generation of antiepileptic drugs and oxidative stress. *Int. J. Mol. Sci.* **2023**, *24*, 3873. https://doi.org/10.3390/ijms24043873.
17. Song, F.; Li, Q.; Wan, Z.Y.; Zhao, Y.J.; Huang, F.; Yang, Q.; Zhao, W.F.; Zhang, M.; Chen, Y.J. Lamotrigine reverses masseter overactivity caused by stress maybe via Glu suppression. *Physiol. Behav.* **2014**, *137*, 25–32. https://doi.org/10.1016/j.physbeh.2014.06.017.
18. Skrzypczak-Wiercioch, A.; Sałat, K. Lipopolysaccharide-induced model of neuroinflammation: Mechanisms of action, research application and future directions for its use. *Molecules* **2022**, *27*, 5481. https://doi.org/10.3390/molecules27175481.
19. Yang, L.; Zhou, R.; Tong, Y.; Chen, P.; Shen, Y.; Miao, S.; Liu, X. Neuroprotection by dihydrotestosterone in LPS-induced neuroinflammation. *Neurobiol. Dis.* **2020**, *140*, 104814. https://doi.org/10.1016/j.nbd.2020.104814.
20. Mani, V.; Arfeen, M. Betahistine's neuroprotective actions against lipopolysaccharide-induced neurotoxicity: Insights from experimental and computational studies. *Brain Sci.* **2024**, *14*, 876. https://doi.org/10.3390/brainsci14090876.
21. Alharbi, B.H.; Alshammari, A.A.A.; Mani, V. Lamotrigine attenuates lipopolysaccharide-induced working-memory impairment and is associated with changes in neuroinflammatory, oxidative-stress, and apoptosis-related markers. *Brain Sci.* **2026**, *16*, 971. https://doi.org/10.3390/brainsci16090971.
22. Percie du Sert, N.; Hurst, V.; Ahluwalia, A.; Alam, S.; Avey, M.T.; Baker, M.; Browne, W.J.; Clark, A.; Cuthill, I.C.; Dirnagl, U.; et al. The ARRIVE guidelines 2.0: Updated guidelines for reporting animal research. *PLoS Biol.* **2020**, *18*, e3000410. https://doi.org/10.1371/journal.pbio.3000410.
23. Fu, X.X.; Duan, R.; Wang, S.Y.; Zhang, Q.Q.; Wei, B.; Huang, T.; Gong, P.Y.; Yan, E.; Jiang, T.; Zhang, Y.D. Lamotrigine protects against cognitive deficits, synapse and nerve cell damage, and hallmark neuropathologies in a mouse model of Alzheimer's disease. *Neural Regen. Res.* **2023**, *18*, 189–193. https://doi.org/10.4103/1673-5374.343888.
24. Wang, K.; Fernandez-Escobar, A.; Han, S.; Zhu, P.; Wang, J.H.; Sun, Y. Lamotrigine reduces inflammatory response and ameliorates executive function deterioration in an Alzheimer's-like mouse model. *BioMed Res. Int.* **2016**, *2016*, 7810196. https://doi.org/10.1155/2016/7810196.
25. Weidner, N.; Semple, J.P.; Welch, W.R.; Folkman, J. Tumor angiogenesis and metastasis--correlation in invasive breast carcinoma. *N. Engl. J. Med.* **1991**, *324*, 1–8. https://doi.org/10.1056/NEJM199101033240101.

26. Morris, G.M.; Huey, R.; Lindstrom, W.; Sanner, M.F.; Belew, R.K.; Goodsell, D.S.; Olson, A.J. AutoDock4 and AutoDockTools4: Automated docking with selective receptor flexibility. *J. Comput. Chem.* **2009**, *30*, 2785–2791. https://doi.org/10.1002/jcc.21256.
27. Trott, O.; Olson, A.J. AutoDock Vina: Improving the speed and accuracy of docking with a new scoring function, efficient optimization, and multithreading. *J. Comput. Chem.* **2010**, *31*, 455–461. https://doi.org/10.1002/jcc.21334.
28. Warren, G.L.; Andrews, C.W.; Capelli, A.-M.; Clarke, B.; LaLonde, J.; Lambert, M.H.; Lindvall, M.; Nevins, N.; Semus, S.F.; Senger, S.; et al. A critical assessment of docking programs and scoring functions. *J. Med. Chem.* **2006**, *49*, 5912–5931. https://doi.org/10.1021/jm050362n.
29. Kontoyianni, M.; McClellan, L.M.; Sokol, G.S. Evaluation of docking performance: Comparative data on docking algorithms. *J. Med. Chem.* **2004**, *47*, 558–565. https://doi.org/10.1021/jm0302997.
30. Cole, J.C.; Murray, C.W.; Nissink, J.W.M.; Taylor, R.D.; Taylor, R. Comparing protein–ligand docking programs is difficult. *Proteins* **2005**, *60*, 325–332. https://doi.org/10.1002/prot.20497.
31. Hopkins, A.L.; Groom, C.R.; Alex, A. Ligand efficiency: A useful metric for lead selection. *Drug Discov. Today* **2004**, *9*, 430–431. https://doi.org/10.1016/S1359-6446(04)03069-7.
32. Wang, S.; Jiang, Y.; Yang, A.; Meng, F.; Zhang, J. The expanding burden of neurodegenerative diseases: An unmet medical and social need. *Aging Dis.* **2025**, *16*, 2937–2952. https://doi.org/10.14336/AD.2024.1071.
33. Geerlings, A.D.; Kapelle, W.M.; Sederel, C.J.; Tenison, E.; Wijngaards-Berenbroek, H.; Meinders, M.J.; Munneke, M.; Ben-Shlomo, Y.; Bloem, B.R.; Darweesh, S.K.L. Caregiver burden in Parkinson's disease: A mixed-methods study. *BMC Med.* **2023**, *21*, 247. https://doi.org/10.1186/s12916-023-02933-4.
34. Wang, J.; Hao, Y.; Ma, D.; Feng, L.; Yang, F.; An, P.; Su, X.; Feng, J. Neurotoxicity mechanisms and clinical implications of six common recreational drugs. *Front. Pharmacol.* **2025**, *16*, 1526270. https://doi.org/10.3389/fphar.2025.1526270.
35. Altahrawi, A.Y.; James, A.W.; Shah, Z.A. The role of oxidative stress and inflammation in the pathogenesis and treatment of vascular dementia. *Cells* **2025**, *14*, 609. https://doi.org/10.3390/cells14080609.
36. Castel-Branco, M.M.; Lebre, V.A.M.; Falcão, A.C.; Figueiredo, I.V.; Caramona, M.M. Relationship between plasma and brain levels and the anticonvulsant effect of lamotrigine in rats. *Eur. J. Pharmacol.* **2003**, *482*, 163–168. https://doi.org/10.1016/j.ejphar.2003.09.065.
37. Walker, M.C.; Tong, X.; Perry, H.; Alavijeh, M.S.; Patsalos, P.N. Comparison of serum, cerebrospinal fluid and brain extracellular fluid pharmacokinetics of lamotrigine. *Br. J. Pharmacol.* **2000**, *130*, 242–248. https://doi.org/10.1038/sj.bjp.0703337.
38. Römermann, K.; Helmer, R.; Löscher, W. The antiepileptic drug lamotrigine is a substrate of mouse and human breast cancer resistance protein (ABCG2). *Neuropharmacology* **2015**, *93*, 7–14. https://doi.org/10.1016/j.neuropharm.2015.01.015.
39. Kwon, H.S.; Koh, S.H. Neuroinflammation in neurodegenerative disorders: The roles of microglia and astrocytes. *Transl. Neurodegener.* **2020**, *9*, 42. https://doi.org/10.1186/s40035-020-00221-2.
40. Wang, L.; Jiao, W.; Wu, J.; Zhang, J.; Tang, M.; Chen, Y. Ulinastatin alleviates early brain injury after intracerebral hemorrhage by inhibiting necroptosis and neuroinflammation via MAPK/NF-κB signaling pathway. *Acta Cir. Bras.* **2022**, *37*, e370301. https://doi.org/10.1590/acb370301.
41. Prabhakaran, J.; Molotkov, A.; Mintz, A.; Mann, J.J. Progress in PET imaging of neuroinflammation targeting COX-2 enzyme. *Molecules* **2021**, *26*, 3208. https://doi.org/10.3390/molecules26113208.
42. Mattson, M.P. Apoptosis in neurodegenerative disorders. *Nat. Rev. Mol. Cell Biol.* **2000**, *1*, 120–129. https://doi.org/10.1038/35040009.
43. Del Duca, F.; Treglia, M.; La Russa, R.; De Simone, S.; Cipolloni, L.; Maiese, A.; Frati, P. Evaluation of apoptotic caspase-3 immunopositivity in human model of asphyxial death. *Int. J. Mol. Sci.* **2025**, *26*, 3317. https://doi.org/10.3390/ijms26073317.
44. Vogler, M.; Braun, Y.; Smith, V.M.; Westhoff, M.A.; Pereira, R.S.; Pieper, N.M.; Anders, M.; Callens, M.; Vervliet, T.; Abbas, M.; et al. The BCL2 family: From apoptosis mechanisms to new advances in targeted therapy. *Signal Transduct. Target. Ther.* **2025**, *10*, 91. https://doi.org/10.1038/s41392-025-02176-0.
45. Dash, U.C.; Bhol, N.K.; Swain, S.K.; Samal, R.R.; Nayak, P.K.; Raina, V.; Panda, S.K.; Kerry, R.G.; Duttaroy, A.K.; Jena, A.B. Oxidative stress and inflammation in the pathogenesis of neurological disorders: Mechanisms and implications. *Acta Pharm. Sin. B* **2025**, *15*, 15–34. https://doi.org/10.1016/j.apsb.2024.10.004.
46. Poljšak, B.; Jamnik, P.; Milisav, I. The importance of multifaceted approach for accurate and comprehensive evaluation of oxidative stress status in biological systems. *Antioxidants* **2025**, *14*, 1083. https://doi.org/10.3390/antiox14091083.
47. Rasheed, Z. Therapeutic potentials of catalase: Mechanisms, applications, and future perspectives. *Int. J. Health Sci. (Qassim)* **2024**, *18*, 1–6.

48. Villalba, N.; Ma, Y.; Gahan, S.A.; Joly-Amado, A.; Spence, S.; Yang, X.; Nash, K.R.; Yuan, S.Y. Lung infection by Pseudomonas aeruginosa induces neuroinflammation and blood-brain barrier dysfunction in mice. *J. Neuroinflammation* **2023**, *20*, 127. https://doi.org/10.1186/s12974-023-02817-7.
49. Walker, D.G.; Lue, L.F. Immune phenotypes of microglia in human neurodegenerative disease: Challenges to detecting microglial polarization in human brains. *Alzheimers Res. Ther.* **2015**, *7*, 56. https://doi.org/10.1186/s13195-015-0139-9.
50. Wu, H.H.; Leng, S.; Eisenstat, D.D.; Sergi, C.; Leng, R. Targeting mutant p53 in cancer: From mechanistic insights to therapeutic strategies. *Cell. Mol. Biol. Lett.* **2026**, *31*, 87. https://doi.org/10.1186/s11658-026-00907-x.
51. Pantsar, T.; Poso, A. Binding affinity via docking: Fact and fiction. *Molecules* **2018**, *23*, 1899. https://doi.org/10.3390/molecules23081899.
52. Roth, B.L.; Sheffler, D.J.; Kroeze, W.K. Magic shotguns versus magic bullets: Selectively non-selective drugs for mood disorders and schizophrenia. Nat. Rev. *Drug Discov.* **2004**, *3*, 353–359. https://doi.org/10.1038/nrd1346.
53. Anighoro, A.; Bajorath, J.; Rastelli, G. Polypharmacology: Challenges and opportunities in drug discovery. *J. Med. Chem.* **2014**, *57*, 7874–7887. https://doi.org/10.1021/jm5006463.
54. Hopkins, A.L.; Keserü, G.M.; Leeson, P.D.; Rees, D.C.; Reynolds, C.H. The role of ligand efficiency metrics in drug discovery. *Nat. Rev. Drug Discov.* **2014**, *13*, 105–121. https://doi.org/10.1038/nrd4163.
55. Rouzer, C.A.; Marnett, L.J. Structural and chemical biology of the interaction of cyclooxygenase with substrates and non-steroidal anti-inflammatory drugs. *Chem. Rev.* **2020**, *120*, 7592–7641. https://doi.org/10.1021/acs.chemrev.0c00215.
56. Lee, H.J.; Ertley, R.N.; Rapoport, S.I.; Bazinet, R.P.; Rao, J.S. Chronic administration of lamotrigine downregulates COX-2 mRNA and protein in rat frontal cortex. *Neurochem. Res.* **2008**, *33*, 861–866. https://doi.org/10.1007/s11064-007-9526-3.
57. Ramadan, E.; Basselin, M.; Rao, J.S.; Chang, L.; Chen, M.; Ma, K.; Rapoport, S.I. Lamotrigine blocks NMDA receptor-initiated arachidonic acid signalling in rat brain: Implications for its efficacy in bipolar disorder. *Int. J. Neuropsychopharmacol.* **2012**, *15*, 931–943. https://doi.org/10.1017/S1461145711001003.
58. Fuentes-Prior, P.; Salvesen, G.S. The protein structures that shape caspase activity, specificity, activation and inhibition. *Biochem. J.* **2004**, *384*, 201–232. https://doi.org/10.1042/BJ20041142.
59. Havran, L.M.; Chong, D.C.; Childers, W.E.; Dollings, P.J.; Dietrich, A.; Harrison, B.L.; Marathias, V.; Tawa, G.; Aulabaugh, A.; Cowling, R.; et al. 3,4-Dihydropyrimido(1,2-a)indol-10(2H)-ones as potent non-peptidic inhibitors of caspase-3. *Bioorg. Med. Chem.* **2009**, *17*, 7755–7768. https://doi.org/10.1016/j.bmc.2009.09.036.
60. Nam, Y.J.; Kim, A.; Lee, M.S.; Shin, Y.K.; Sohn, D.S.; Lee, C.S. Lamotrigine attenuates proteasome inhibition-induced apoptosis by suppressing the activation of the mitochondrial pathway and the caspase-8- and Bid-dependent pathways. *Neurochem. Res.* **2016**, *41*, 2503–2516. https://doi.org/10.1007/s11064-016-1962-5.
61. Mureddu, L.G.; Vuister, G.W. Fragment-based drug discovery by NMR. Where are the successes and where can it be improved? *Front. Mol. Biosci.* **2022**, *9*, 834453. https://doi.org/10.3389/fmolb.2022.834453.
62. Oltersdorf, T.; Elmore, S.W.; Shoemaker, A.R.; Armstrong, R.C.; Augeri, D.J.; Belli, B.A.; Bruncko, M.; Deckwerth, T.L.; Dinges, J.; Hajduk, P.J.; et al. An inhibitor of Bcl-2 family proteins induces regression of solid tumours. *Nature* **2005**, *435*, 677–681. https://doi.org/10.1038/nature03579.
63. Souers, A.J.; Leverson, J.D.; Boghaert, E.R.; Ackler, S.L.; Catron, N.D.; Chen, J.; Dayton, B.D.; Ding, H.; Enschede, S.H.; Fairbrother, W.J.; et al. ABT-199, a potent and selective BCL-2 inhibitor, achieves antitumor activity while sparing platelets. *Nat. Med.* **2013**, *19*, 202–208. https://doi.org/10.1038/nm.3048.
64. Leng, Y.; Fessler, E.B.; Chuang, D.M. Neuroprotective effects of the mood stabilizer lamotrigine against glutamate excitotoxicity: Roles of chromatin remodelling and Bcl-2 induction. *Int. J. Neuropsychopharmacol.* **2013**, *16*, 607–620. https://doi.org/10.1017/S1461145712000429.
65. He, M.M.; Smith, A.S.; Oslob, J.D.; Flanagan, W.M.; Braisted, A.C.; Whitty, A.; Cancilla, M.T.; Wang, J.; Lugovskoy, A.A.; Yoburn, J.C.; et al. Small-molecule inhibition of TNF-alpha. *Science* **2005**, *310*, 1022–1025. https://doi.org/10.1126/science.1116304.

Disclaimer/Publisher's Note: The statements, opinions and data contained in all publications are solely those of the individual author(s) and contributor(s) and not of MDPI and/or the editor(s). MDPI and/or the editor(s) disclaim responsibility for any injury to people or property resulting from any ideas, methods, instructions or products referred to in the content.